

Frontiers in Science and Engineering International Journal

Edited by The Hassan II Academy of Science and Technology of Morocco

Mathematics, Applied Mathematics, Computer Sciences

Contents

- i **WELCOME**
- ii **Foreword**
- 1 **In Memorium**
- 5 **Golden Mean, Fractals and Islamic Geometric Patterns**
Aziz KHAMJANE and Rachid BENSLIMANE
- 17 **Multi-Level Kernel-Based QAM Symbol Error Probability Estimation**
Pasteur Poda and Samir Saoudi
- 29 **Efficient Use of the Spectrum in Small Cell Deployments for 5G Wireless Communications Networks**
Sandra Lagen, Adrian Agustin, and Josep Vidal
- 45 **The Hassan mosque at the digital era.**
Farouk Achakir, Marc Pierrrot Deseilligny, Sanaa El Fkihi, Mina El Mghari, Mohamed Ettarid, El Mustapha Mouaddib and Amina Radgui

Editorial board

Editor-in-Chief :

O. FASSI-FEHRI, Permanent Secretary, Hassan II Academy of Science and Technology, Morocco

Associate Editors-in-Chief :

M. BOUSMINA, Chancellor, Hassan II Academy of Science and Technology, Morocco

J. DERCOURT, Honorary Permanent Secretary, Académie des Sciences, France

C. GRISCELLI, Université René Descartes, France

D. OUAZAR, Université Mohammed VI Polytechnique, Benguerir (Executive director)

Associate Editors :

Mathematics. Applied Mathematics. Computer Sciences

G. GAMBOLATTI, Università Degli Studi di Padova, Italy

M. GHALLAB, Institut National de Recherche en Informatique et en Automatique (INRIA), France

Y. OUKNINE, Faculté des Sciences, Université Cadi Ayyad - Marrakesh, Morocco

E. ZUAZUA, Basque Center for Applied Mathematics, Bilbao, Spain

Physics. Chemistry. Engineering Sciences

D. AIT KADI, Laval University, Canada

A. BENYOUSSEF, Faculté des Sciences, Université Mohammed V, Rabat, Morocco

M. BOUSMINA, Chancellor, Hassan II Academy of Science and Technology, Morocco

E.M. ESSASSI, Faculté des Sciences, Université Mohammed V, Rabat, Morocco

G.G. FULLER, Stanford University, California, USA

A. MAAZOUZ, Institut National de Sciences Appliquées, Lyon, France

D. OUAZAR, Université Mohammed VI Polytechnique, Benguerir

E.H. SAIDI, Faculté des Sciences, Université Mohammed V, Rabat, Morocco

P.A. TANGUY, Ecole Polytechnique - Montréal (Canada)

Life Sciences (Medical. Health. Agriculture. Biology. Genetics)

T. CHKILI, Faculté de Médecine, Université Mohammed V, Rabat, Morocco

R. EL AOUAD, Faculté de Médecine, Université Mohammed V, Rabat, Morocco

C. GRISCELLI, Institut Necker, Faculté de Médecine, Université René Descartes, France

A. SASSON, GID, Paris, France

A. SEFIANI, Institut National d'Hygiène, Rabat, Morocco

Earth. Water and Oceans. Environmental Sciences

M. AIT KADI, Conseil Général du Développement Agricole, Rabat, Morocco

A. CHENG, University of Mississippi, USA

A. EHI ASSANI, Institut Scientifique, Rabat, Morocco

R.T. HANSON, USGS, USA

T. OUARDA, INRS-Eau, Canadas

M.S. VASCONCELOS, EU Fisheries, Portugal

Strategic Studies and Economic Development

N. ELAOUFI, Faculté des Sciences Juridiques, Economiques et Sociales, Université Mohammed V, Rabat, Morocco

M. BERRIANE, Chercheur au labomtoira mixte international MediTer, Morocco

K. SEKKAT, Université Libre de Bruxelles, Belgique

Frontiers in Science and Engineering International Journal

Edited by The Hassan II Academy of Science and Technology of Morocco

Mathematics, Applied Mathematics, Computer Sciences

Contents

- i **WELCOME**
- ii **Foreword**
- 1 **In Memorium**
- 5 **Golden Mean, Fractals and Islamic Geometric Patterns**
Aziz KHAMJANE and Rachid BENSLIMANE
- 17 **Multi-Level Kernel-Based QAM Symbol Error Probability Estimation**
Pasteur Poda and Samir Saoudi
- 29 **Efficient Use of the Spectrum in Small Cell Deployments for 5G Wireless Communications Networks**
Sandra Lagen, Adrian Agustin, and Josep Vidal
- 45 **The Hassan mosque at the digital era.**
Farouk Achakir, Marc Pierrot Deseilligny, Sanaa El Fkihi, Mina El Mghari, Mohamed Ettarid, El Mustapha Mouaddib and Amina Radgui

Dépôt légal : 2012 PE 0007
ISSN : 2028 - 7615

ACADEMY Press MA

Email : fse@academiesciences.ma
www.academiesciences.ma/fse/

Layout by : AGRI-BYS S.A.R.L (A.U)
Printed by : Imprimerie LAWNE
11, rue Dakar, 10040 - Rabat

WELCOME TO FSE

Frontiers in Science and Engineering, an International Journal edited by The Hassan II Academy of Science and Technology uses author-supplied PDFs for all online and print publication.

The objective of this electronic journal is to provide a platform of exchange of high quality research papers in science and engineering. Though it is rather of wide and broad spectrum, it is organized in a transparent and simple interactive manner so that readers can focus on their direct interest.

All papers are submitted to the normal peer-review process. Publication criteria are based on :

i) Novelty of the problem or methodology and problem solving, **ii)** Saliency of the approach and solution technique, **iii)** Technical correctness and outputs, **iv)** Clarity and organization.

Papers are first reviewed by the Executive Board Director who receives the paper and, if relevant in terms of the overall requirements, it is then proposed to one of the most appropriate associate editor on the field who will select 2 to 3 expert reviewers. Electronic printing will allow considerable time savings for submission delays which will be reduced drastically to less than three to six months. Prospective authors are therefore invited to submit their contribution for assessment while subjected to similar quality criteria review used in paper journals.

Authors are notified of acceptance, need for revision or rejection of the paper. It may be noted that papers once rejected cannot be resubmitted. All the details concerning the submission process are described in another section. This electronic journal is intended to provide :

- the announcement of significant new results,
- the state of the art or review articles for the development of science and technology,
- the publication of proceedings of the Academy or scientific events sponsored by the Academy,
- the publication of special thematic issues.

So that the scientific community can :

- promptly report their work to the scientific community,
- contribute to knowledge sharing and dissemination of new results.

The journal covers the established disciplines, interdisciplinary and emerging ones. Articles should be a contribution to fundamental and applied aspects, or original notes indicating a significant discovery or a significant result.

The topics of this multidisciplinary journal covers amongst others :

Materials Science, Mathematics, Physics, Chemistry, Computer sciences, Energy, Earth Science, Biology, Biotechnology, Life Sciences, Medical Science, Agriculture, Geosciences, Environment, Water, Engineering and Complex Systems, Science education, Strategic and economic studies, and all related modeling, simulation and optimization issues, etc. ...

Once, a certain number of papers in a specific thematic, is reached, the Academy might edit a special paper issue in parallel to the electronic version.

FOREWORD

The present volume of “Frontiers in Sciences and Engineering” is a special issue dedicated to the memory of our friend and colleague Driss ABOUTAJJEDINE, born on February 2, 1966 and who passed away on August 31, 2015.

Upon his sudden death, late Driss ABOUTAJDINE was the Director of the National Research Council of Morocco, and Professor (Head of ILRIT Laboratory, Faculty of Science - Rabat, U) and Vice-President at the two Universities of Rabat and resident member (since May2006) of the Hassan II Academy of Sciences and Technology. He was very active in research and has made several important contributions related to computational aspects and applications to signal processing, automatic learning, image recognition, embedded systems communications, simulation frameworks for IT amongst others.

The authors of the articles in this volume are colleagues and friends of Driss ABOUTAJDINE. Through their contributions, they wish to pay tribute to him. All the papers have been evaluated positively by peer referees.

Papers cover a wide range of research activities within the field of expertise Driss ABOUTAJDINE

The Editors

In Memorium



Pr. Driss ABOUTAJDINE (30/12/1953 - 04/03/2017)

بسم الله الرحمن الرحيم

”من المؤمنين رجال صدقوا ما عاهدوا الله عليه فمنهم من قضى نحبه ومنهم من ينتظر وما بدلوا تبديلاً“
صدق الله العظيم.

Le Samedi 4 mars 2017, nous avons appris avec une profonde affliction et une grande tristesse le décès de notre confrère le Professeur Driss Aboutajdine, membre résident de l'Académie Hassan II des Sciences et Techniques depuis son installation solennelle le 18 mai 2006 par Sa Majesté Le Roi, que Dieu Le protège, au Palais Royal d'Agadir, après une courte maladie qu'il a affrontée avec un courage et une lucidité exceptionnels. Notre tristesse est toujours aussi profonde que celle ressentie ce jour triste que fut le 4 mars dernier. En cette douloureuse circonstance, nous renouvelons au nom de tous les membres de l'Académie Hassan II des Sciences et Techniques à l'ensemble des membres de l'honorable famille du défunt, à son épouse et à ses enfants, à ses proches et à ses amis, ainsi qu'à sa grande famille scientifique, en particulier les membres de notre Compagnie, nos vives condoléances dans cette cruelle épreuve, ainsi que nos sincères sentiments de compassion. La perte de notre regretté collègue Driss Aboutajdine fut la perte d'un grand homme et d'un grand scientifique du Maroc contemporain; nous implorons Le Tout-Puissant de l'entourer de Sa miséricorde et de Sa clémence, et de l'accueillir dans Son vaste paradis parmi les élus vénérables, et d'accorder aux membres de sa famille patience, consolation et réconfort.

M. Driss Aboutajdine est né le 30 décembre 1953. Il a obtenu sa Licence en Physique à la Faculté des Sciences de Rabat en 1976. Comme étudiant, il a été parmi les brillants éléments que chaque enseignant souhaite avoir dans sa classe ou son amphithéâtre. Après avoir obtenu sa Licence, notre regretté défunt a été parmi ceux qui ont choisi de poursuivre leurs études supérieures et opté pour une carrière d'enseignant-chercheur. Après son CEA en Informatique et Traitement du Signal, obtenu en 1977, il a continué ses études et a soutenu sa thèse de 3^{ème} cycle (DES) en 1980, puis son Doctorat d'Etat Es-Sciences à l'Université Mohammed V-Agdal en 1985 à l'âge de 32 ans.

Il a commencé sa carrière d'enseignant-chercheur très jeune. Recruté à l'âge de 25 ans en tant qu'Assistant à la Faculté des Sciences de Rabat, il a ensuite exercé comme Maître-assistant, puis Maître de Conférences et Professeur de l'enseignement supérieur à la même Faculté.

Au cours de sa carrière professionnelle, le regretté Driss Aboutajdine a été à plusieurs reprises professeur-chercheur invité dans plusieurs institutions d'enseignement supérieur et de recherche en Europe dont Suptelecom Paris, Université de Bordeaux 1, Université de Rouen, Université de Nantes et Université Polytechnique de Catalogne et en Amérique du Nord dont Université du Sud du Massachusetts, MIT et Université de Stanford.

Ce qui distingue le défunt dans sa carrière professionnelle c'est surtout son parcours de chercheur. Il fût d'abord directeur du Laboratoire de Recherche en Informatique et Télécommunications à la Faculté des Sciences de Rabat, puis coordonnateur national du pôle de compétences «Sciences et Technologies de l'Information et de la Communication» (STIC) qui regroupe plus de 30 laboratoires et équipes de recherche universitaires et plusieurs partenaires industriels; il convient de rappeler qu'il fût l'un des membres d'IEEE depuis 1988 et senior member depuis 1999. Il a aussi lancé la série de colloques «International Symposium on Signal, Image, Video and Communication» (ISIVC), dont il présidait son comité de pilotage, à Rabat en 2000, à Brest en 2004, à Tunis en 2006 et à Bilbao en 2008, et les conférences «International Conference on Image and Signal Processing» à Agadir en 2001 et «International Symposium on Communications, Control and Signal Processing» (ISCCSP) à Marrakech en 2006.

Le défunt Pr. Driss Aboutajdine a contribué aussi à la formation par la recherche en dirigeant et en encadrant un nombre important de doctorats dont certains préparés en cotutelle avec des collègues d'universités françaises, espagnoles ou nord américaines. Il est aussi membre du comité éditorial de plusieurs revues internationales dont la revue «Traitement du signal» et le journal «Eurasip Journal on Image and Video Processing». Il a été également membre du comité de lecture de plusieurs conférences et revues internationales et auteur ou co-auteur de plusieurs publications scientifiques dans des conférences et journaux scientifiques nationaux et internationaux. Ses domaines d'intérêt comprennent le traitement de l'information multimédia et les télécommunications.

Maîtrisant parfaitement sa discipline scientifique, Driss Aboutajdine restera un grand enseignant-chercheur et un grand scientifique dans le domaine du traitement de l'information et des télécommunications au Maroc.

Sur le plan de la production scientifique, la base de données SCOPUS, consultée le 8 mars 2017, indique qu'entre 2000 et 2017 le Pr. Driss Aboutajdine a co-signé 396 publications scientifiques (63% Conference paper; 35% Article;...), essentiellement en Computer Science (47%), en Engineering (29%) et en Mathématiques (15%). Ces publications ont été citées 1029 fois, avec un H-index de 15.

En plus de sa qualité de grand professeur, de chercheur confirmé et de producteur scientifique de haut niveau, notre regretté défunt a occupé le poste de Vice-président de l'Université Mohammed V-Agdal et Vice-président de l'Université Mohammed V-Souissi. En 2013, il fût nommé par le Chef du Gouvernement, Directeur du Centre National pour la Recherche Scientifique et Technique, et en 2014, il fût nommé par Sa Majesté le Roi, Membre du Conseil Supérieur de l'Education, de la Formation et de la Recherche Scientifique.

Le 18 mai 2006, sa carrière scientifique fût couronnée par sa nomination par Sa Majesté le Roi comme Membre résident au sein de l'Académie Hassan II des Sciences et Techniques. Depuis sa nomination au sein de notre Compagnie, la contribution personnelle du Pr. Aboutajdine, son aide précieuse, sa réflexion et sa disposition lors de la mise en œuvre des missions de l'Académie, notamment dans le cadre des activités de ses organes directeurs et surtout du Collège Sciences de la Modélisation et de l'Information, dont il a été le premier directeur et un membre dynamique, et au sein duquel ses activités ont été particulièrement importantes et précieuses; l'Académie restera à jamais reconnaissante.

Le regretté Pr. Driss Aboutajdine a été parmi les premiers membres élus des organes directeurs de l'Académie. Dès la première session plénière solennelle inaugurale qui a permis à l'Académie de mettre en place ses organes directeurs, le regretté Pr. Driss Aboutajdine a été élu membre du premier Conseil d'Académie (2006-2007) et fut aussi élu premier directeur du Collège des Sciences de la Modélisation et de l'Information (2006-2007). Par la suite, il a été élu Directeur des Séances (2010-2011) et membre de la Commission des Travaux (2015-2016).

Homme de sciences d'une grande ouverture d'esprit, le Pr. Driss Aboutajdine était aussi membre de l'Académie des Sciences Africaine et de l'Académie des Sciences du Tiers Monde (TWAS). Il était également promu «Chevalier des palmes académiques» en France et récipiendaire des insignes d'Officier de l'Ordre National du Mérite de la République Française.

Malgré sa notoriété qui impressionne comme un grand Professeur, notre regretté Pr. Aboutajdine a été aussi un ardent défenseur de la recherche scientifique et du développement technologique. Il croyait fermement à l'importance de la science et de la technologie dans le développement du pays.

Sur le plan humain, il reste un grand scientifique et un grand humaniste. Il est connu pour sa simplicité, sa courtoisie, son engagement, son dévouement pour ses étudiants et s'émerveillant devant leurs réussites. Il a été pour eux toujours accueillant et disponible, les traitant comme des égaux, des collaborateurs et toujours prêt à les aider à s'engager et à les conseiller dans leur vie professionnelle.

Avec le décès du Pr. Driss Aboutajdine, notre Académie a perdu un de ses membres résidents parmi les plus éminents. Elle a perdu en lui un grand homme dont les qualités scientifiques et humaines étaient faites de noblesse, de grandeur d'âme, de patience dans l'épreuve, de clairvoyance, de pondération, de rectitude et de sagacité. Dynamique, attentif aux autres, toujours animé du sens du bien commun et des intérêts de son pays. Il a marqué de son empreinte les dix premières années de notre Académie. Il était pour nous un pilier, un soutien et un homme qui forçait le respect par sa rigueur, sa pudeur et par une humilité marquée de simplicité et de modestie. Autour de sa personnalité nous sommes unanimes à donner en exemple sa probité, son honnêteté, sa loyauté et son patriotisme.

La disparition de Pr. Driss Aboutajdine est une énorme perte pour notre pays et pour notre Académie, et le vide qu'il laisse ne sera à jamais comblé. Il restera dans nos mémoires comme un chercheur de talent et un scientifique particulièrement imaginatif et exigeant, dont les contributions à la promotion de la recherche et de la science dans notre pays resteront bien vivantes et auront marqué sur le plan national notre SSI (Système scientifique et d'innovation).

C'est dire tout le vide que le regretté Pr. Driss Aboutajdine laisse derrière lui au niveau de ses proches certes, mais aussi au niveau de cette grande famille composée des hommes et des femmes scientifiques qui croient comme lui que le développement de notre pays passe par la formation, l'éducation, la recherche scientifique, la liberté et la culture.

Nous implorons Dieu, Tout-Puissant, d'accueillir le défunt dans son vaste paradis parmi les Prophètes, les Saints, les martyrs et les vertueux et lui accorder une ample rétribution pour les efforts louables et les bonnes œuvres qu'il a accomplies au service de son pays et de sa famille.

En ces circonstances douloureuses, nous tenons de nouveau à exprimer nos condoléances les plus attristées à sa famille et plus particulièrement à son épouse et à ses enfants et l'ensemble de ses amis en implorant le Tout Puissant d'avoir le défunt en Sa Sainte Miséricorde.

«Nous sommes à Dieu et à Lui nous retournons».

Golden Mean, Fractals and Islamic Geometric Patterns

Aziz KHAMJANE and Rachid BENSLIMANE

Laboratoire de Transmission et de Traitement de l'Information, Ecole Supérieure de Technologie,
Université Sidi Mohamed Ben Abdellah, route d'Imouzzer, FEZ, 30000, Morocco
Corresponding author, E-mail: khamjane.aziz@gmail.com; rachid.benslimane@usmba.ac.ma

Abstract. *Islamic Geometric art has received a great attention from several scientists and designers. Hence, several investigations have been done to reveal its secret of construction, to analyze its symmetry and to prove that some patterns are periodic or quasi-periodic. Our investigation in this paper takes a different way from existing researches. It consists of discovering some aspects of beauty related to the mathematical properties, such as the golden mean, of this art by analyzing an historical pattern. Findings of this analyze will be used to design and develop new geometric patterns.*

Key words: Islamic art, Rosette, Golden mean, Islamic star patterns, Fractals

1. Introduction

Islamic geometric art is a kind of Islamic decoration, where Muslims craftsmen have excelled in the use of geometric lines to create wonderful patterns. The forms such as: polygons, stars, and overlapping circles are used in decorating buildings, wood and copper artifacts, doors and ceilings. The beauty and complexity of this art have attracted several researchers to investigate it. Therefore, several works have been done to analyze the symmetry of Islamic geometric patterns [1]–[4] and to reveal the secret of their construction [5]–[18]. Also, a great debate is opened about the presence of the quasi-periodicity in Islamic geometric patterns [19]–[25]. In this work, we will first investigate the ten folds pattern of the Attarine Madrassa (Fez) (Fig1). Then, we will analyze the design elements used in Islamic geometric art (stars and rosettes) with regard to the golden mean. Then, we will present a technique to design a new variety of Islamic geometric patterns in the proportions of the golden mean. Finally, we will describe a method to create nearly fractal Islamic geometric patterns.

2. Golden mean

The golden mean $\left(\frac{1+\sqrt{5}}{2}\right)$ is a special number approximately equal to 1,618. It is designated by the Greek letter ϕ (phi) in homage to the Greek sculptor Phidias (born about 490 and died around 430 BC). The golden ratio comes up in nature and in architectural buildings such as the great pyramid of Giza (Egypt) and the Parthenon in Athens (Greece) [26]. In the twelfth century, the mathematician Leonardo Fibonacci discovered a recurrent mathematical sequence. This sequence was present in nature and is called the Fibonacci sequence [27]. We will show that many patterns of Islamic geometric art are claimed to have been designed using the golden ratio.

3. Islamic geometric art

Islamic ornamentation consists of three types: floral designs, calligraphy and geometric patterns. It occurs in rich profusion throughout Islamic cultures. It is found on a diversity of materials and many types of objects. The last category (geometric patterns) is one of the most distinguishing features of Islamic art. Islamic star patterns are the most beautiful in Geometric patterns [2]. They are the result of repeated copies of symmetric shapes that resemble to a 'star' or 'rosette'. The star and rosette shapes with 6, 8, 10, 12 and 16 rays are the most frequent.

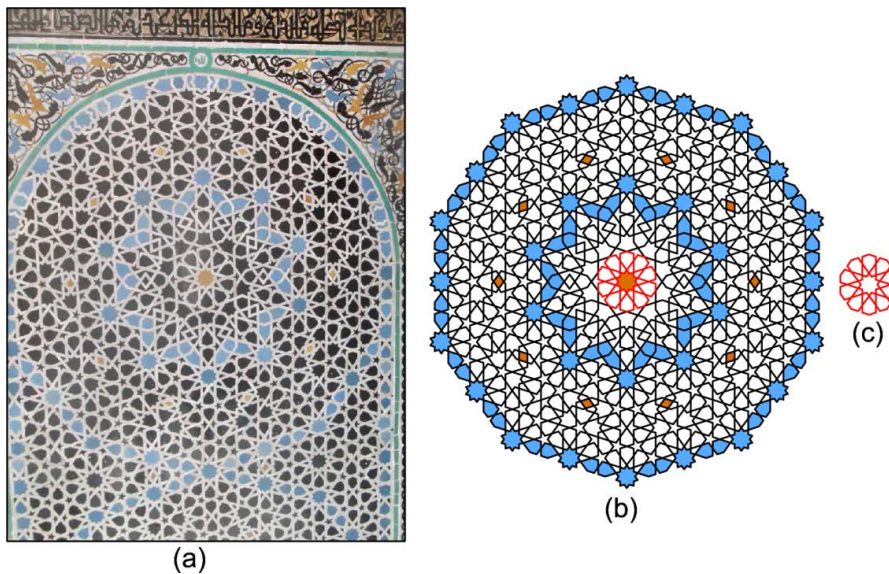


Figure 1 the pattern that adorns the panel of the Madrasa Attarine in Fez, Morocco (a), a constructed cartwheel of the pattern (b), the 10-rayed rosette which contained in the pattern.

4. Design Element

As mentioned in the previous section, Islamic star patterns are the result of repeated copies of stars or rosettes. A star is an arrangement of line segments which can be defined by the following parameters (N, R, θ, S) (Fig .2):

N: Is the order of the star.

R: Is the radius of the star.

θ : Is the angle made by the segment DG and the side of the regular surrounding polygon.

S: Is the number of intersections of each edge of the star with others.

Besides the parameters described above, the rosette can be defined by the angle: $\beta = \widehat{GBH}$ (Fig. 2.) A Construction of ‘ideal’ rosette is described in [28].

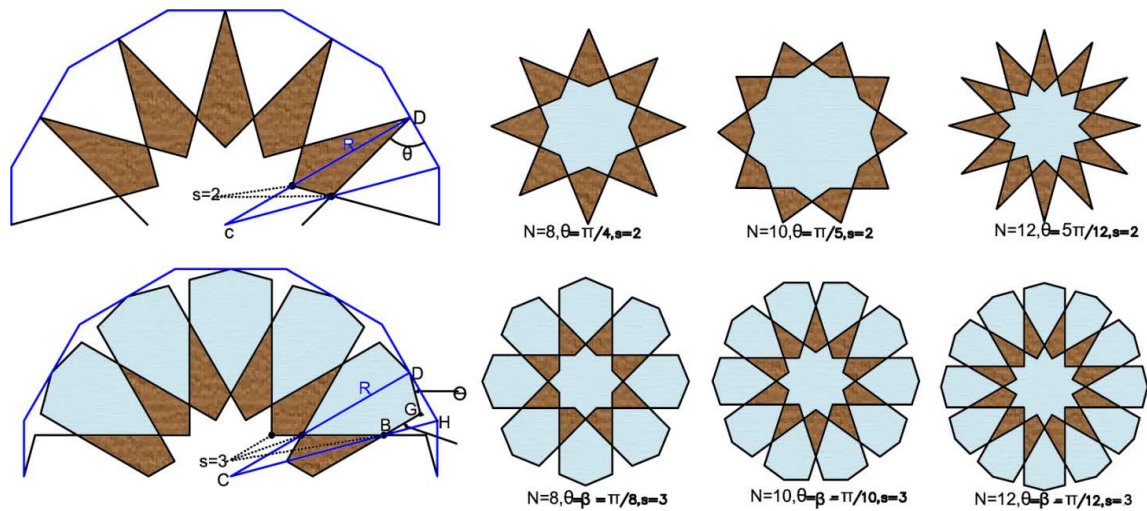


Figure 2 The parameters of the star and rosette with several examples of stars and rosettes.

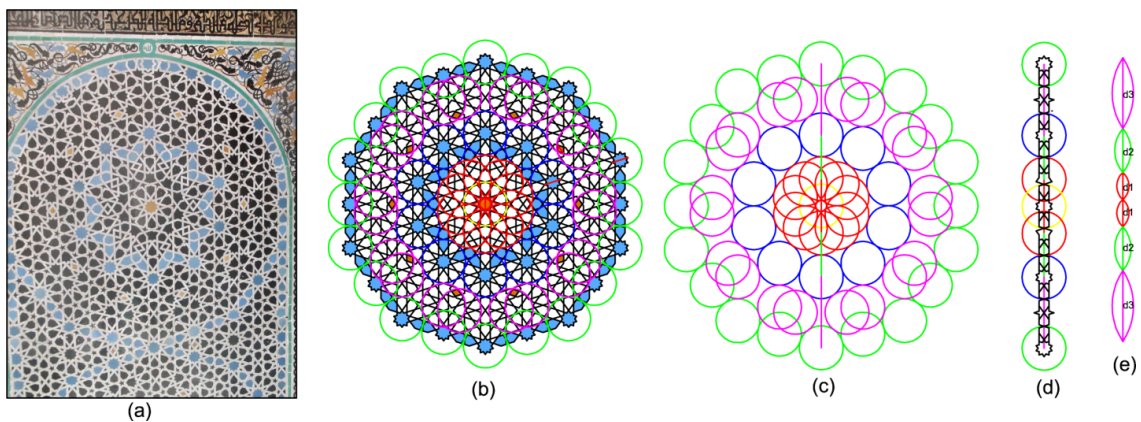


Figure 3 Panel of Madrassa Attarine (Fez Morocco) (a), distribution of rosettes (b), distribution of circles surrounding rosette (c), distance between collinear centers of consecutive circles (d)(e).

5. Analysis of the pattern of the panel of the madrassa Attarine (FEZ morocco).

The pattern of the panel of the Attarine Madrasa is a result of repeated copies of 10-rayed rosettes (complete and incomplete 10-rayed rosettes). These copies are distributed around the complete 10-rayed rosette in the center. To understand this distribution, we replace each rosette (complete or incomplete rosette) by a circle that surrounds it. The result of this distribution is shown in Fig 3 (c). The examination of the distances between collinear centers of consecutive rosettes (Fig 3(d)(e)) shows that these distances are in the ratio of the golden mean: $\frac{d_3}{d_2} = \frac{d_2}{d_1} = \varphi$.

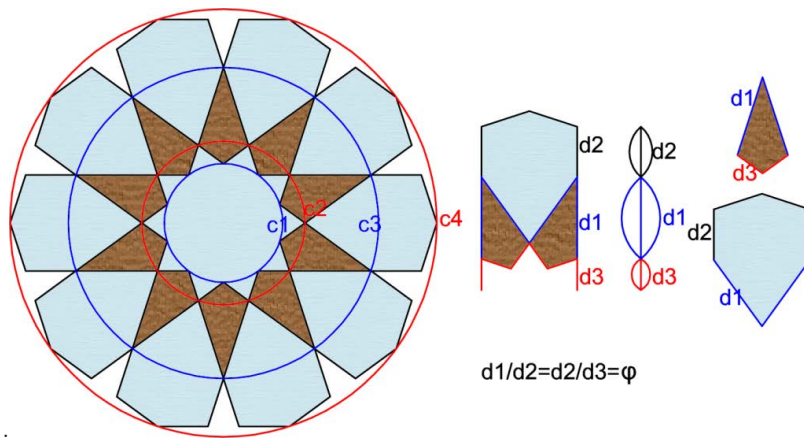


Figure 4 Properties of a ten-pointed rosette with parameters $(\theta = \beta = \frac{\pi}{10}, s = 3)$ rosette in relation to the golden mean.

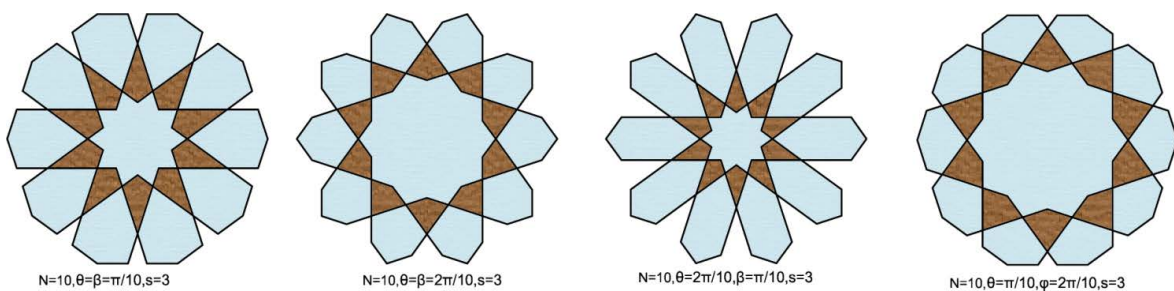


Figure 5 Different forms of ten-pointed rosettes with their associated parameters.

6. The 10-rayed rosette exudes the golden ratio

Figure 4 illustrates several examples of 10-rayed rosette with different parameters (θ, β). If you are asked to choose the most beautiful rosette among those in Figure 4; you will often choose, as me, the first one which used in the panel analyzed above. Maybe you do not know the secret of this beauty! It is the golden mean. Let's us unveil this secret. The examination of the lengths of the segments extracted from the rosette with the parameters: $(N = 10, \theta = \beta = \frac{\pi}{10}, s = 3)$ shows that are in the ratio of the golden mean (Fig 5): $\frac{d_1}{d_2} = \varphi$, $\frac{d_1}{d_3} = \varphi^2$ and $\frac{d_1}{d_2} = \frac{d_2}{d_3} = \varphi$. In addition to that, as illustrated in figure 4, the radii of the concentric blue and red circles are in the ratio of golden mean: $\frac{R_{C_3}}{R_{C_1}} = \frac{R_{C_4}}{R_{C_2}} = \varphi^2$.

An "extended rosette" [10] is obtained by extending and joining up the edges from adjacent tips of the rosette. The extended 10-rayed rosette with the same parameters described above is shown in figure 6 where the golden mean comes up also. The second extension of the rosette revealed the kite used in the Penrose tiling and other proportions of the golden mean.

The examination of 10-rayed star with the parameters: $(\theta = \frac{3\pi}{10}, s = 2)$, shows that the lengths of the segments are in the golden ratio. The extracted shape is exactly the kite used in the Penrose tiling.

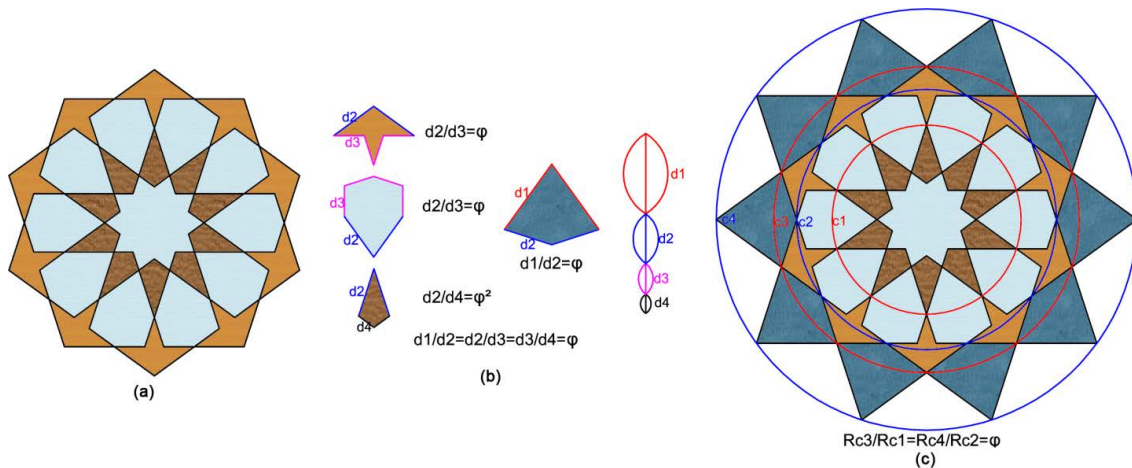


Figure 6 Extended 10-rayed rosette (a), the shapes forming the extended rosette and their proportions. The kite used in the Penrose tiling comes up (the dark blue shape) (b), (c) an extended rosette obtained by extending the outer edges of the extended rosette in (a).

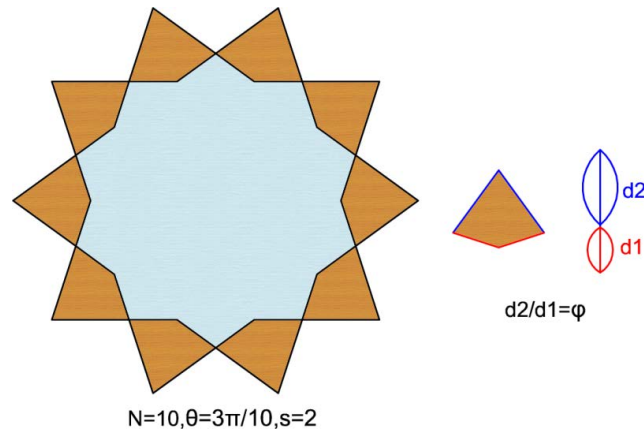


Figure 7 a 10-pointed star.

7. Construction of patterns with the golden mean

As showed in the analysis of the pattern of the Madrassa Al Attarine in Fez, the rosettes are distributed according to the golden mean. To obtain a pattern where the rosettes are distributed according to the golden ratio, we must begin by elaborating an underlying sub-grid which determines the centers of the rosettes. The underlying sub-grid will contain circles that represent the rosettes of the patterns.

We begin by reconstructing the pattern analyzed in Figure 1. A regular rosette is inserted in each copy of the red circles in Figure 8. b. The blue circles will contain a 10-pointed rosette with a little modification of two petals (Figure 8. c). For the overlapping circles, we place a portion of the rosette in the own part of each circle (Figure 8 .d) and we fill the overlapping area using a specific formation of this pattern (Figure 8 .e).

To construct new patterns, we begin by distributing 10 points evenly along the perimeter of concentric circles of radii R_1 , R_2 and R_3 where $R_3/R_2 = R_2/R_1 = \phi$ Figure 9(a).

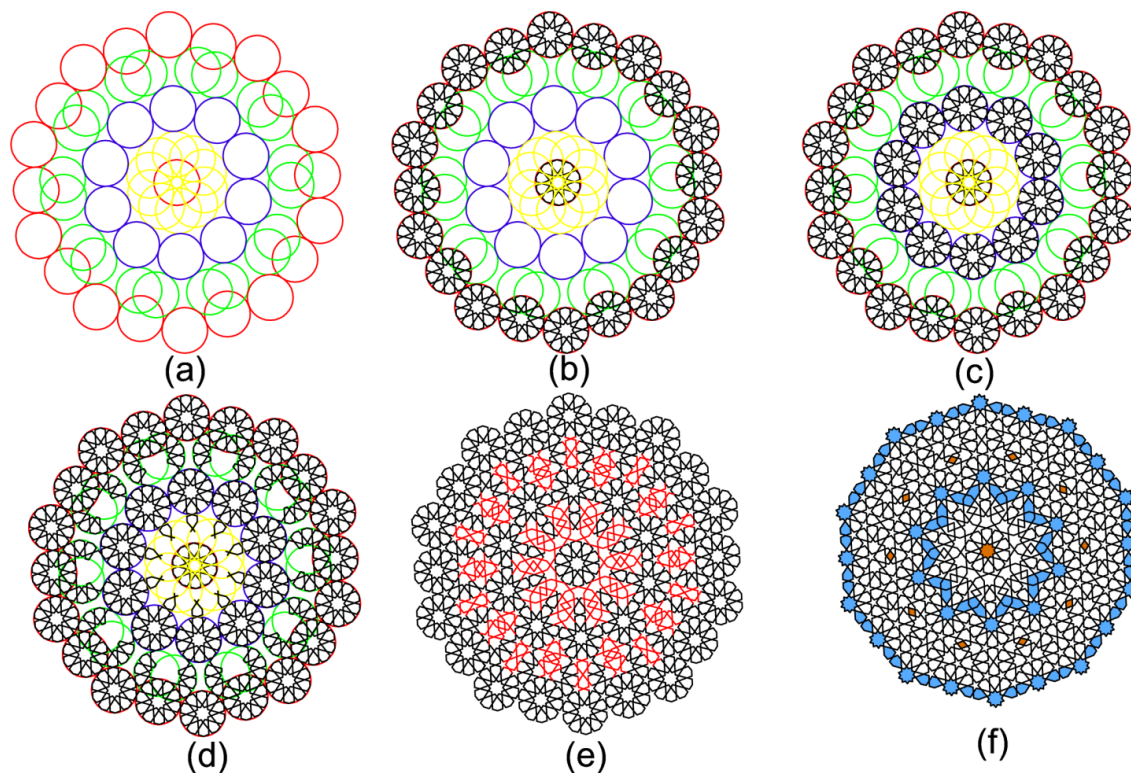


Figure 8 Reconstruction of the pattern of the panel of the Madrasa Attarine in FEZ.

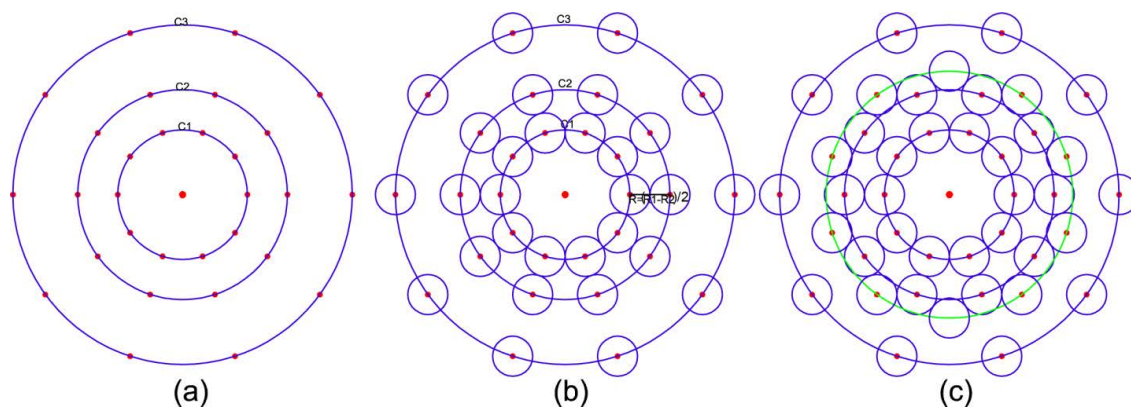


Figure 9 Construction of the sub-grid.

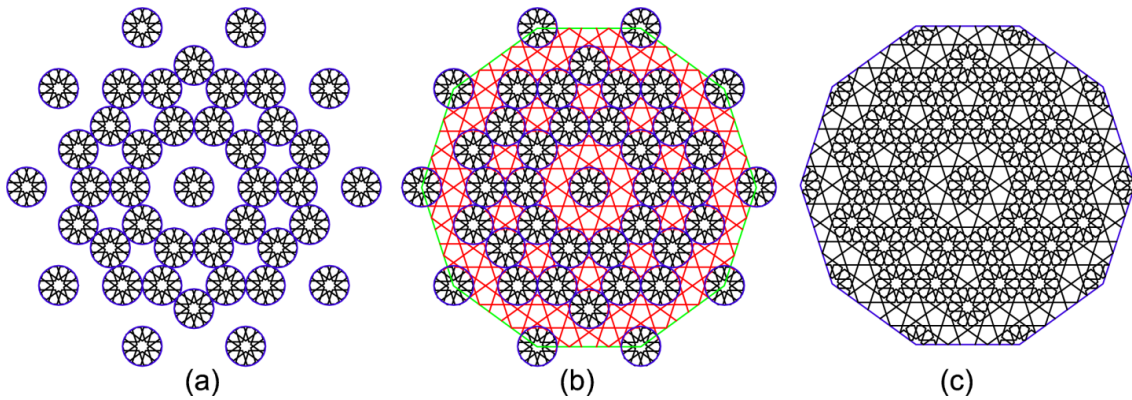


Figure 10 Construction of a new pattern with 10-pointed rosette distributed according to the golden mean.

The radius of the circumscribed circles of the rosettes is determined by the equation: $R = (R_{c2} - R_{c1})/2$ Figure 9. (b). An additional circle is inserted between the C2 and C3 circles to minimize the distance between them (Figure 9. (c)). Ten points will be distributed evenly along the perimeter of the additional circle. These points are not aligned the others points and make an angle of $\frac{\pi}{10}$ with them. The rosettes of the patterns are inserted within the circles (Figure 10. (a)), and the interstitial area is covered by extending the line segments Figure 10. (b). The examination of the obtained pattern (Figure 10. (c)), shows that it is made up of the shapes illustrated in Figure 11. These shapes are made up of line segments of four different lengths d_1, d_2, d_3, d_4 where $\frac{d_4}{d_3} = \frac{d_3}{d_2} = \frac{d_2}{d_1} = \varphi$.

To obtain another pattern we can distribute the points (centers of rosettes) in different manner. In Figure 12(a), five points are distributed evenly along the perimeters of the C1 and C2 circles and ten points are distributed evenly along the perimeters of the two remaining circles.

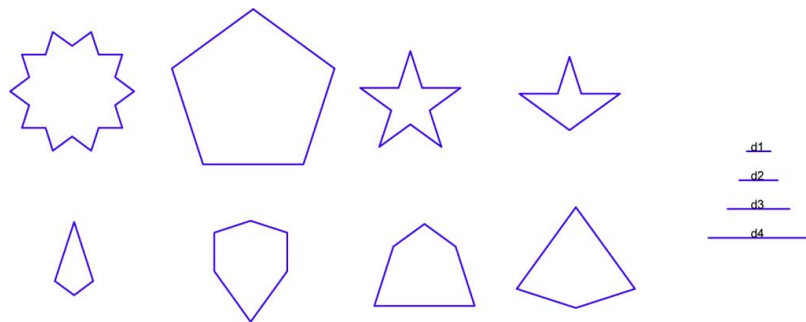


Figure 11 The extracted geometric shapes of the constructed pattern in Figure 10(c).

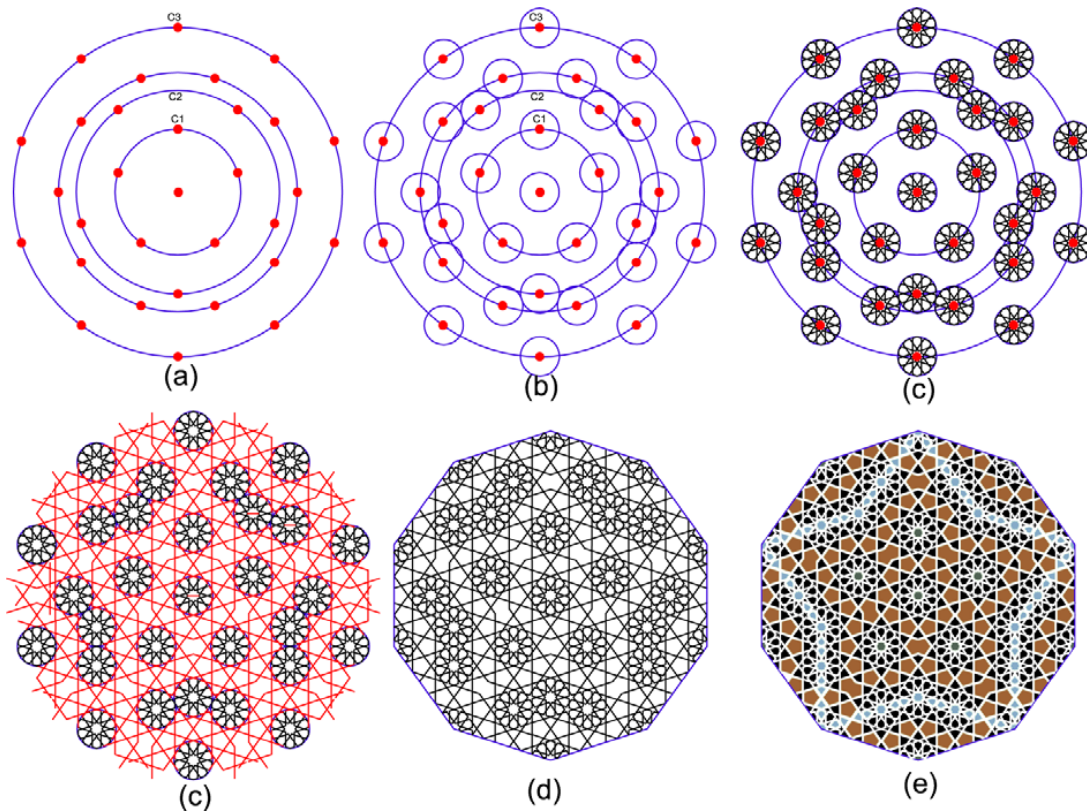


Figure 12 Construction of another pattern by using different distribution of the rosettes.

8. Construction of nearly fractal patterns

A Fractal is infinitely complex pattern that is self-similar across different scales. It is created by repeating a simple process over and over in an ongoing feedback loop. Geometrically, they exist in between our familiar dimensions. Fractal patterns are extremely familiar, since nature is full of fractals. For instance: trees, rivers, coastlines, mountains, clouds, seashells, hurricanes, etc. However, it is not easy to design a Fractal Islamic geometric pattern because of the properties of Islamic geometric patterns. One of these properties is that each vertex of the pattern is a bivalent or a 4-valent vertex. Each 4-valent vertex of the pattern must fit the requirement of the perfect crossing. In this section we will show the process of creating a nearly fractal patterns with respect to the properties of Islamic geometric patterns. We use two rosettes where the ratio of their radii is in the golden mean. Ten copies of the small rosette will be distributed evenly along the perimeters of the blue circles (Figure 13 .a). The ratio of the blue circles is in φ^2 . The greater rosette will be distributed evenly along the perimeter of the red circles where the ratio of the radii is in the golden mean (Figure 13). The remaining steps are similar to those illustrated in the previous circles and shown in Figure 13. In Figure 14, another pattern is obtained by using a different distribution of circles. The ratio of the radii of the blue concentric circles is in φ^2 and the ratio of the radii of the red circles is in φ^3 .

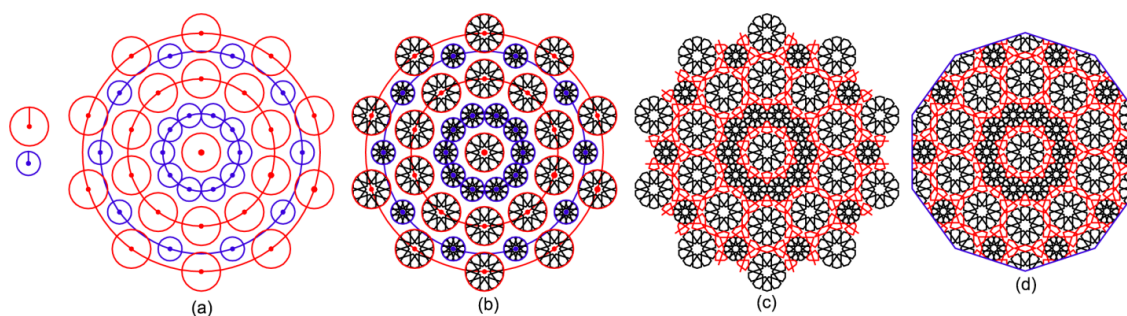


Figure 13 Construction of Islamic geometric pattern with 10-pointed rosettes where the ratio of the radii is in the golden mean.

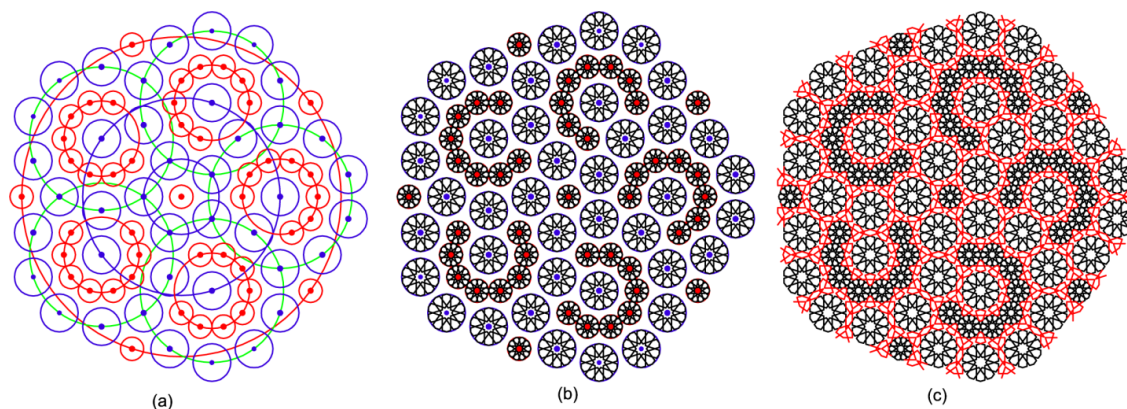


Figure 14 Construction of geometric pattern with two 10-pointed rosettes where the ratio of the radii is in the golden mean.

9. Conclusion

This work have taken a different way from the majority of researches and investigated Islamic geometric patterns in relation to the golden mean to show some aspects of its beauty. We have demonstrated the presence of the golden mean in Islamic art by analyzing the pattern of the Madrassa Attarine (Fez, Morocco). For the design element (star and rosette) we have determined the parameters that lead to the apparition of the golden mean as the proportion between the segment lengths of the motif. Findings of this analysis have been used to construct several new patterns with the golden mean proportions and nearly fractal patterns. This work opens another way of investigating Islamic geometric patterns in order to create beautiful patterns that explore the golden mean and the fractal geometry in the construction and the distribution of the stars/rosettes.

References

- [1] B. Grünbaum and G. C. Shephard, "Interlace Patterns in Islamic and Moorish Art," *Leonardo*, vol. 25, no. 3, pp. 331–339, 1992.
- [2] S. J. Abas and A. S. Salman, *Symmetries of Islamic Geometrical Patterns*. 1995.
- [3] S. J. Abas and A. S. Salman, "Geometric and Group-Theoretic Methods for Computer Graphic Studies of Islamic Symmetric Patterns," *Comput. Graph. Forum*, vol. 11, no. 1, pp. 43–53, 1992.

- [4] M. O. Djibril and R. O. H. Thami, "Islamic geometrical patterns indexing and classification using discrete symmetry groups," *J. Comput. Cult. Herit.*, vol. 1, no. 2, pp. 1–14, 2008.
- [5] E. H. Hankin, "Examples of methods of drawing geometrical arabesque patterns," *Math. Gaz.*, vol. 12, pp. 371–373, 1925.
- [6] E. H. Hankin, "The drawing of geometric patterns in saracenic art," in *Memoirs of Archaeological Survey of India*, vol. 15, 1925.
- [7] E. H. Hankin, "Some difficult Saracenic de-signs II," *Math. Gaz.*, vol. 18, pp. 165–168, 1934.
- [8] E. H. Hankin, "Some difficult Saracenic designs III," *Math. Gaz.*, vol. 20, pp. 318–319, 1936.
- [9] C. S. Kaplan, "Islamic star patterns from polygons in contact," *Proc. 2005 Conf. Graph. Interface*, pp. 177–185, 2005.
- [10] C. S. Kaplan, "Computer generated islamic star patterns," *Bridges*, pp. 105–112, 2000.
- [11] C. S. Kaplan and D. H. Salesin, "Islamic star patterns in absolute geometry," *ACM Trans. Graph.*, vol. 23, no. 2, pp. 97–119, 2004.
- [12] A. . Dewdney, "The Tinkertoy Computer and Other Machinations," in *The Tinkertoy Computer and Other Machinations*, W. H. Freeman, Ed. 1993, pp. 222–230.
- [13] V. Ostromoukhov, "Mathematical Tools for Computer-generated Ornamental Patterns," in *7th International Conference on Electronic Publishing*, 1998, pp. 193–223.
- [14] J. Bonner, "The design of particularly complex non-systematic geometric patterns with multiple centers of localized symmetry," in *les tracés de l'arabesque géométrique*, Fondation de la mosquée Hassan II de Casablanca, Ed. Casablanca, 2014, pp. 85–94.
- [15] M. Castera, Jean, *Arabesques: Decorative Arts in Morocco*, ACR Editio. 1996.
- [16] P. R. Cromwell, "A modular design system based on the Star and Cross pattern," *J. Math. Arts*, vol. 6, no. 1, pp. 29–42, 2012.
- [17] P. R. Cromwell, "Islamic Geometric Designs from the Topkapı Scroll I : Unusual Arrangements of Stars," *J. Math. Arts*, vol. 4, no. 2, pp. 73–85, 2010.
- [18] J. Bonner, "The historical use of polygonal systems to create islamic geometric patterns," in *les tracés de l'arabesque géométrique*, Fondation de la mosquée Hassan II de Casablanca, Ed. Casablanca, 2014, pp. 85–94.
- [19] E. Makovicky, "800-year-old pentagonal tiling from Maragha, Iran, and the new varieties of aperiodic tiling it inspired," in *Fivefold symmetry*, Singapore-New Jersey etc.: World Scientific Publishing Co Pte Ltd, 1992, pp. 67–86.
- [20] E. Makovicky, F. R. Pérez, and P. F. Hach-Alí, "Decagonal patterns in the Islamic ornamental art of Spain and Morocco," *Bol. la Soc. Esp. Mineral.*, vol. 21, pp. 107–127, 1998.
- [21] E. Makovicky and N. M. Makovicky, "The first find of dodecagonal quasiperiodic tiling in historical Islamic architecture," *J. Appl. Crystallogr.*, vol. 44, no. 3, pp. 569–573, 2011.
- [22] P. R. Cromwell, "The search for quasi-periodicity in islamic 5-fold ornament," *Math. Intell.*, vol. 31, no. 1, pp. 36–56, 2009.
- [23] P. R. Cromwell, "Cognitive Bias and Claims of Quasiperiodicity in Traditional Islamic Patterns," *Math. Intell.*, vol. 37, no. 4, pp. 30–44, 2015.
- [24] Y. Aboufakil, A. Thalal, and M. A. E. I. Raghni, "Moroccan ornamental quasiperiodic patterns constructed by the multigrid method," *J. Appl. Crystallogr.*, vol. 47, no. 2, pp. 630–641, 2014.
- [25] J. Bonner and M. Pelletier, "A 7-Fold System for Creating Islamic Geometric Patterns Part 1 : Historical Antecedents," pp. 141–148, 2012.
- [26] G. Meisner, "The Parthenon and Phi, the Golden Ratio," 2013. [Online]. Available: <http://www.goldennumber.net/parthenon-phi-golden-ratio/>.
- [27] A. S. Posamentier and I. Lehmann, *The (Fabulous) Fibonacci Numbers*. Prometheus Books, 2007.
- [28] E. Lee, J, "islamique star paterms," *Muqarnas*, vol. 4, pp. 182–197, 1987.

Multi-Level Kernel-Based QAM Symbol Error Probability Estimation

Pasteur PODA^{1,3} and Samir SAOUDI²

¹ Université Nazi BONI, 01 BP 1091 Bobo-Dioulasso 01, Burkina Faso

² IMT Atlantique Bretagne-Pays de la Loire, Lab-Sticc UMR 6285, Brest, France

³ Corresponding author, E-mail: pasteur.poda@univ-bobo.bf

Abstract. *Kernel density estimators technique has been successfully applied to efficient Bit Error Rate (BER) computation issue under a diversity of simulation frameworks. However, as contemporary and emerging digital communication systems are increasingly provided with advanced transceivers, it is questionable if the Symbol Error Rate (SER) can be anyway derived from the BER. This paper investigates for a direct way to efficiently compute the SER. Focusing on the ubiquitous multi-level Quadrature Amplitude Modulation (QAM) transmission schemes, a Gaussian kernel-based estimator is designed. Simulation of the 4-QAM transmission scheme under various channel models shows that the proposed estimator can achieve efficient estimations with a very high degree of accuracy and reliability.*

Key words: kernel density estimators, probability density function estimation, bit error probability estimation, symbol error probability estimation.

1. Introduction

The issue of efficient error probability estimation for the performance evaluation of digital communication systems has been an active subject of research during the 1970s. Attempts to establish analytical methods of Bit Error Probability (BEP) estimation have been noted [1], [2] but did not meet success. However, simulation-based techniques rapidly showed to be more successful. In [3], a complete review dealt in details with simulation-based techniques namely the standard Monte Carlo (MC) simulation and variance-reducing techniques such as importance sampling (also called modified Monte Carlo) [4], extreme-value theory [5], tail extrapolation [6] and quasi-analytical estimation [3].

The standard MC technique is the most general of all existing simulation-based techniques of error probability estimation. Indeed, this technique does not need to be adapted to the communication system specificities. It is an intuitive and easy way to compute an estimate of the error

probability. It makes a comparison between the transmitted and the received data sequences and then proceeds with the errors counting. The error rate, an estimate of the error probability, is then derived as the ratio of the number of observed errors to the total size of the transmitted sequence. So, the standard MC appears to be a universal technique for the computation of Bit Error Rate (BER) or Symbol Error Rate (SER). Unfortunately, it is revealed to be the most costly computation of error rate simulation methods [3]. To achieve a given level of accuracy and reliability, the standard MC can require large sample size causing the computational cost to be increasingly high whilst the error rate to compute gets smaller.

To overcome the standard MC method computational cost, the family of variance-reducing techniques and more specifically the importance sampling technique has been well investigated. Very high efficiency of factor theoretically going up to hundreds were reported regarding the importance sampling technique. However, this most successful variance-reducing technique requires a prior knowledge about the underlying probability density function (pdf) of the observations based on which the estimation is made. A more recent approach for efficient error probability estimation consists of using kernel density estimators [7], [8].

The approach based on kernel density estimators allows the error rate to be computed without requiring any prior knowledge about the underlying pdf of the observations. The pdf of soft observations, i.e., those observations sampled from the channel output and serving for hard decision making about the transmitted symbols, is estimated in a non-parametric manner using a kernel density estimator. Then, based on a selected kernel density estimator, some mathematical manipulations allow an equation of the error probability estimate to be derived. Finally, using soft observations at the receiver-end, the estimate of the error probability is computed by simulation.

The first works related to kernel-based error probability estimation dealt with the BER computation. They include works reported in [9], [10] and to some extent, that work [11] based on Parzen's pdf estimator. Parzen's pdf estimator is a more general class that includes kernel estimators. The latest kernel-based BEP estimation works were reported in [12] and [13]. Otherwise, investigations dealing with Symbol Error Probability (SEP) estimation led to results reported in [14] and [15]. Herein, this paper aims at extending the work presented in [15]. The BEP and the SEP are two parameters commonly used in digital communications domain for systems performance evaluation. For Gray coded mappings over the usual channels and for large ranges of signal to noise ratios, it is mathematically demonstrated that the SEP estimate (i.e., the SER) can be deduced from the BEP estimate (i.e., the BER) and inversely [16]. However, in the contemporary and emerging digital communication systems characterised by advanced and complex transceivers, it is questionable if the SER can be anyway deduced from the BER. Far from answering this question, the purpose of this paper is to offer a direct and efficient approach to compute the SER in any digital communication system where the Quadrature Amplitude Modulation (QAM) schemes take place.

In the remainder of this paper, we first formalise in Section 2 the SEP as a function of the pdf of the received soft observations. We then present in Section 3 the SEP estimate based on the kernel density estimators approach. From the general design of the M -QAM SEP estimate made in Section 3, we define in Section 4 the special case of 4-QAM SEP estimator. We specify in Section 5 the simulation frameworks, report and analyse the simulation results. Finally, we conclude the paper in Section 6.

2. Formal Symbol Error Probability

To formulate the SEP estimation problem, let us consider a digital communication system with rectangular M -QAM (4-QAM, 16-QAM, 64-QAM, etc.) constellations. Let $(s_i)_{1 \leq i \leq N}$ be a set of N independent and identically distributed information symbols. Each s_i takes its value into the alphabet of waveforms $\{S_1, S_2, \dots, S_M\}$. At the receiver-end, we assume the presence of soft symbols which are noisy copies of the transmitted symbols s_i . Let us denote by Z , the multivariate Random Variable (RV) describing the received soft observations, such as $Z = (X, Y)$ where X and Y are real RVs. Let $(Z_i)_{1 \leq i \leq N}$ be the sequence of the realisations of Z where each $Z_i = (X_i, Y_i)$ corresponds to the soft decision statistic that serves for the computation of the hard decision about the transmitted information symbol s_i . Let us assume a clustering of the received soft observations Z_i into M clusters $(C_m)_{1 \leq m \leq M}$; each with cardinality N_m . Then, the *a priori* probability that the transmitted symbol s_i is equal to S_m is

$$\pi_m \triangleq Pr[s_i = S_m], \tag{2.1}$$

where $m \in \{1, 2, \dots, M\}$, $Pr[\cdot]$ denotes the probability of a given event and $\pi_1 + \pi_2 + \dots + \pi_M = 1$. The soft observations $(Z_i)_{1 \leq i \leq N}$ are RVs having the same pdf $f_{Z,N}(x, y)$. The pdf $f_{Z,N}(x, y)$ is a mixture of M marginal multivariate conditional pdfs and is given by

$$f_{Z,N}(x, y) = \sum_{m=1}^M \pi_m f_{Z,N_m}^{S_m}(x, y), \tag{2.2}$$

where $f_{Z,N_m}^{S_m}(x, y)$ is the conditional multivariate pdf of Z_i conditional to $s_i = S_m$. The SEP is therefore given by:

$$p_{e,N} = \sum_{m=1}^M \pi_m p_{e,N_m}, \tag{2.3}$$

where,

$$p_{e,N_m} = 1 - \iint_{\mathcal{D}_m} f_{Z,N_m}^{S_m}(x, y) dx dy, \tag{2.4}$$

where $\mathcal{D}_m = \{Z \mid m = \underset{1 \leq k \leq M}{\operatorname{argmin}} d(Z, S_k)\}$, with $d(\cdot, \cdot)$ denoting the euclidian distance, is the decision-region associated to S_m .

3. Gaussian Kernel-Based M -QAM SEP Estimation

In this Section, we proceed with a general formulation, based on the kernel density estimators, of the M -QAM SEP estimation problem. We establish a general expression of the Gaussian kernel-based SEP estimate for any M -QAM transmission scheme.

As shown in equations (2.3) and (2.4), the analytical expressions of the marginal conditional pdfs $f_{Z,N_1}^{S_1}(x, y)$, $f_{Z,N_2}^{S_2}(x, y)$, \dots , $f_{Z,N_M}^{S_M}(x, y)$ are required to compute the SEP $p_{e,N}$. Unfortunately, these conditional pdfs depend on the communication channel model and receiver scheme so that their exact parametric model is not always available. However, it is possible to resort to a non-parametric estimation technique such as the kernel density estimators. Therefore, let us denote by $\hat{f}_{Z,N_m}^{S_m}(x, y)$ the kernel-based estimate of the marginal multivariate pdf $f_{Z,N_m}^{S_m}(x, y)$. Then, the kernel method allows $\hat{f}_{Z,N_m}^{S_m}(x, y)$ to be written as follows,

$$\hat{f}_{Z,N_m}^{S_m}(x, y) = \frac{1}{N_m} \sum_{Z_i \in C_m} \frac{1}{h_{N_m}^x} K\left(\frac{x - X_i}{h_{N_m}^x}\right) \times \frac{1}{h_{N_m}^y} K\left(\frac{y - Y_i}{h_{N_m}^y}\right), \tag{3.1}$$

where $h_{N_m}^x$ (resp. $h_{N_m}^y$) is the smoothing parameter depending on the soft values X_1, X_2, \dots, X_{N_m} (resp. Y_1, Y_2, \dots, Y_{N_m}) that are associated with those soft observations Z_1, Z_2, \dots, Z_{N_m} which are classified into the cluster C_m . The clusters $(C_m)_{1 \leq m \leq M}$ are the result of a classification procedure. Each cluster C_m is assumed containing the soft observations Z_1, Z_2, \dots, Z_{N_m} which likely belong to the decision-region D_m . The function $K(\cdot)$ is any pdf, called the kernel, assumed to be an even and regular function with zero mean and unit variance.

From (2.3) and (2.4) in which we insert the expressions of the marginal conditional pdfs estimates, we can derive the SEP estimate $\hat{p}_{e,N}$ as follows,

$$\hat{p}_{e,N} = \sum_{m=1}^M \hat{\pi}_m \hat{p}_{e,N_m}, \tag{3.2}$$

where \hat{p}_{e,N_m} , the marginal SEP, is given by

$$\hat{p}_{e,N_m} = 1 - \iint_{D_m} \hat{f}_{Z,N_m}^{S_m}(x, y) dx dy. \tag{3.3}$$

Since rectangular QAM constellations are considered, the decision-regions $(D_m)_{1 \leq m \leq M}$, are such as $D_m = [a_m, b_m] \times [c_m, d_m]$. Then, taking into account the expression of $\hat{f}_{Z,N_m}^{S_m}(x, y)$ as given in (3.1), we get

$$\hat{p}_{e,N_m} = 1 - \frac{1}{N_m} \sum_{Z_i \in C_m} \left\{ \int_{a_m}^{b_m} \frac{1}{h_{N_m}^x} K\left(\frac{x - X_i}{h_{N_m}^x}\right) dx \right\} \times \left\{ \int_{c_m}^{d_m} \frac{1}{h_{N_m}^y} K\left(\frac{y - Y_i}{h_{N_m}^y}\right) dy \right\}. \tag{3.4}$$

Using the changes of variables such as $u = (x - X_i)/h_{N_m}^x, v = (y - Y_i)/h_{N_m}^y$ and setting $\alpha_m = (a_m - X_i)/h_{N_m}^x, \beta_m = (b_m - X_i)/h_{N_m}^x, \gamma_m = (c_m - Y_i)/h_{N_m}^y$ and $\xi_m = (d_m - Y_i)/h_{N_m}^y$, we get

$$\hat{p}_{e,N_m} = 1 - \frac{1}{N_m} \sum_{Z_i \in C_m} \left\{ \int_{\alpha_m}^{+\infty} K(u) du - \int_{\beta_m}^{+\infty} K(u) du \right\} \times \left\{ \int_{\gamma_m}^{+\infty} K(v) dv - \int_{\xi_m}^{+\infty} K(v) dv \right\}. \tag{3.5}$$

From this general expression of \hat{p}_{e,N_m} given by (3.5), if a Gaussian kernel function is selected, then K is a zero mean unit variance Gaussian distribution. A general expression of the Gaussian kernel-based SEP estimate for any M -QAM transmission scheme is therefore expressed as in (3.2) with in addition the following more convenient expression of \hat{p}_{e,N_m} :

$$\hat{p}_{e,N_m} = 1 - \frac{1}{N_m} \sum_{Z_i \in C_m} \left\{ Q\left(\frac{a_m - X_i}{h_{N_m}^x}\right) - Q\left(\frac{b_m - X_i}{h_{N_m}^x}\right) \right\} \times \left\{ Q\left(\frac{c_m - Y_i}{h_{N_m}^y}\right) - Q\left(\frac{d_m - Y_i}{h_{N_m}^y}\right) \right\}, \tag{3.6}$$

where the function $Q(\cdot)$ is the complementary unit cumulative Gaussian distribution and is such as $Q(u) = \int_u^{+\infty} (1/\sqrt{2\pi}) \exp(-t^2/2) dt$.

4. Kernel-Based 4-QAM SEP Estimator

A kernel-based error probability estimator is completely defined by the selection of the kernel function K and its smoothing parameter. The selection of the kernel function can be guided by the density function under estimation. For instance, infinite support distributions such as the Gaussian distribution are suitable as kernel functions whenever the observed samples are distributed over a large scale. Finite support distributions also exist. Further information about them can be found in [17]. The selection of the smoothing parameter is generally concerned with more labor. It has been proven in [8] that the pdf estimation accuracy mainly depends on it. It is also noticed [17] that there is no universal smoothing parameter; i.e., every case of study should accommodate with the judicious method of the optimal smoothing parameter selection. A multitude of methods have been developed for this purpose. Some of them are used in [18] and [19]. A complete review covering these methods can be found in [17]. Several kernel-based BEP estimators (e.g., [9] and [10]) have been built based on the Gaussian kernel.

By the general expression of the SEP estimate given by (3.2) and (3.6), we design a Gaussian kernel-based SEP estimator for any M -QAM transmission scheme except that the smoothing parameters $h_{N_m}^x$ and $h_{N_m}^y$ are not selected yet. Thus, to complete the estimator design and proceed herein with its evaluation in the special case of the 4-QAM transmission scheme, we choose the smoothing parameters as defined in [10] and given by:

$$\begin{cases} h_{N_m}^x = \left(\frac{4}{3}\right)^{\frac{1}{5}} N_m^{-1/5} \sigma_{N_m}^x \\ h_{N_m}^y = \left(\frac{4}{3}\right)^{\frac{1}{5}} N_m^{-1/5} \sigma_{N_m}^y, \end{cases} \tag{4.1}$$

where $(\sigma_{N_m}^x)^2$ (resp. $(\sigma_{N_m}^y)^2$) is the variance of the soft values X_1, X_2, \dots, X_{N_m} (resp. Y_1, Y_2, \dots, Y_{N_m}). In [15], we reported simulation results of an SEP estimator based on the smoothing parameter of (4.1) and provided illustrations of performance regarding 4-QAM and 16-QAM transmission schemes. Without any loss of generality, we'll focus the performance evaluation of the proposed kernel-based SEP estimator on the 4-QAM transmission scheme. In this particular case, the decision-regions are such as: $\mathcal{D}_1 = [0, +\infty[\times [0, +\infty[$, $\mathcal{D}_2 = [0, +\infty[\times]-\infty, 0]$, $\mathcal{D}_3 =]-\infty, 0] \times]-\infty, 0]$ and $\mathcal{D}_4 =]-\infty, 0] \times [0, +\infty[$. Thus, from (3.6), $Q((a_m - X_i)/h_{N_m}^x) = 1$ and $Q((c_m - Y_i)/h_{N_m}^y) = 1$ as $a_m \rightarrow -\infty$ and $c_m \rightarrow -\infty$ respectively. In the same way, $Q((b_m - X_i)/h_{N_m}^x) = 0$ and $Q((d_m - Y_i)/h_{N_m}^y) = 0$ as $b_m \rightarrow +\infty$ and $d_m \rightarrow +\infty$ respectively. Finally as $1 - Q(x) = Q(-x)$, we get from (3.6) the expressions of $(\hat{p}_{e,N_m})_{1 \leq m \leq 4}$ as follows,

$$\left\{ \begin{aligned} \hat{p}_{e,N_1} &= 1 - \int_0^{+\infty} \int_0^{+\infty} \hat{f}_{Z,N_1}^{S_1}(x, y) dx dy \\ &= 1 - \frac{1}{N_1} \sum_{Z_i \in \mathcal{C}_1} Q\left(-\frac{X_i}{h_{N_1}^x}\right) Q\left(-\frac{Y_i}{h_{N_1}^y}\right) \\ \hat{p}_{e,N_2} &= 1 - \int_0^{+\infty} \int_{-\infty}^0 \hat{f}_{Z,N_2}^{S_2}(x, y) dx dy \\ &= 1 - \frac{1}{N_2} \sum_{Z_i \in \mathcal{C}_2} Q\left(-\frac{X_i}{h_{N_2}^x}\right) Q\left(\frac{Y_i}{h_{N_2}^y}\right) \\ \hat{p}_{e,N_3} &= 1 - \int_{-\infty}^0 \int_{-\infty}^0 \hat{f}_{Z,N_3}^{S_3}(x, y) dx dy \\ &= 1 - \frac{1}{N_3} \sum_{Z_i \in \mathcal{C}_3} Q\left(\frac{X_i}{h_{N_3}^x}\right) Q\left(\frac{Y_i}{h_{N_3}^y}\right) \\ \hat{p}_{e,N_4} &= 1 - \int_{-\infty}^0 \int_0^{+\infty} \hat{f}_{Z,N_4}^{S_4}(x, y) dx dy \\ &= 1 - \frac{1}{N_4} \sum_{Z_i \in \mathcal{C}_4} Q\left(\frac{X_i}{h_{N_4}^x}\right) Q\left(-\frac{Y_i}{h_{N_4}^y}\right) \end{aligned} \right. \tag{4.2}$$

5. Simulation Results

5.1. Simulation Frameworks

According to (3.6), the M -QAM SEP estimation using kernel method requires a classification of the soft observations $(Z_i)_{1 \leq i \leq N}$ into as many clusters C_m as the modulation order M . In this paper, we made the classification in a supervised fashion, i.e., the transmitted information sequence is known. The supervised classification procedure consists of the synchronisation of the received sequence positionwise with the transmitted sequence. Then, each observation Z_i of the current index is classified into the cluster assigned to its corresponding information symbol s_i of the same index.

Three types of channel models are considered: the Additive White Gaussian Noise (AWGN) channel, a frequency-selective channel and a frequency-selective Rayleigh fading channel. When the transmissions are made over the AWGN channel, the received soft observations that are used for the SEP estimation are in the form of $Z_i = s_i + \eta_i$, where η_i is a realisation of the channel noise η and $\eta \sim \mathcal{N}(0, \sigma_\eta^2)$.

The frequency-selective channel is one of the frequency-selective channel models designed in [20]. It is defined by a finite impulse response filter h with 11 coefficients. The soft observations used for the SEP estimation are taken from the channel output. They are in the form of $Z_i = \sum_{k=1}^{11} h_k s_{i-k} + \eta_i$. As this channel introduces inter-symbol interferences, an equalisation is made; afterwards the equalised soft observations are used for the SEP estimation.

The third type of channel involved in the simulation of the proposed kernel-based SEP estimator is a multi-carrier frequency-selective Rayleigh fading channel. The profile of this latter type channel is given by: a Gray-labeled 4-QAM constellations, ten taps long with a sample period of $12.8 \mu s$, an $8 Hz$ maximum Doppler shift and average taps gains given in *watts* by the vector $[0.0616 \ 0.4813 \ 0.1511 \ 0.0320 \ 0.1323 \ 0.0205 \ 0.0079 \ 0.0778 \ 0.0166 \ 0.0188]$ [20], [21]. To mitigate the inter-symbol and inter-carrier interferences, we implemented an orthogonal frequency division multiplexing technique of 128 sub-carriers with a cyclic prefix of length 9 [22].

5.2. Numerical Results

The accuracy and the reliability of the proposed kernel-based SEP estimator is analysed using absolute biases and confidence intervals. The absolute bias is for evaluating how accurate is an estimate of the SEP. It is defined by $|\mathbb{E}[\hat{p}_{e,N}] - p_{e,N}|$ where $\mathbb{E}[\cdot]$ denotes the mathematical expectation operator. The Confidence Interval (CI) is for the measure of the estimation reliability. In [3], it has been preferred to variance. To compute $\mathbb{E}[\hat{p}_{e,N}]$ and the CIs, we were provided with 101 SEP estimations trials. Based on the 101 SEP estimates values, the Student's t-distribution method was applied to determine the CIs values for a confidence level of 95%. To complete the absolute bias values calculation, we needed to be provided with values of the SEP $p_{e,N}$. So, when AWGN or Rayleigh fading channels are considered, a theoretical expression of the SEP is available. However, in the case of the frequency-selective channel, the SEP is determined in the form of a benchmark. The benchmark was computed by simulations using the standard MC method under the constraint that a threshold of one hundred errors occurred. Simulations were carried out for different values of the information bit energy to noise power spectral density ratio (E_b/N_0). They covered SER values slightly greater than 10^{-1} down to small SER values: in the vicinity of 10^{-4} when the Rayleigh fading channel is involved and in the vicinity of 10^{-5} regarding the AWGN and the frequency-selective channels.

Figure 1 shows the curve of performance given by the proposed SEP estimator over the AWGN channel. Represented by the curve in solid blue line with diamond mark at each data point, the SEP estimates achieved by the proposed estimator are compared to the theoretical SEP values borne by the curve in red solid line. Following the same legend (i.e., solid blue line with diamond mark at each data point for the proposed estimator and solid red line for the reference curve), Figure 2 and Figure 3 also show the estimation performance achieved over the frequency-selective and the Rayleigh fading channels respectively. These three figures have in common that their plots allow the proposed SEP estimator accuracy to be visually evaluated. The observed SEP estimates as borne by Figure 1, Figure 2 and Figure 3 correspond to the absolute bias numerical data given in the third columns of Table 1, Table 2 and Table 3 respectively. As these tables let us see, the absolute bias values are negligible compared to the true values $p_{e,N}$. This explain why, as the curves in the figures look like, quite all the SEP estimates data points appear pointwise consistent. The resulting accuracy of the SEP estimations is therefore very high.

Beyond the demonstrated high accuracy of the SEP estimations, let us now analyse their reliability. For this, the CIs values characterising the achieved reliability are given in the fourth columns of Table 1, Table 2 and Table 3. The smaller the CI is, more reliable is the SEP estimate. Throughout Table 1, Table 2 and Table 3, the achieved CIs are very small: most of them are close to $[0.9p_{e,N}, 1.1p_{e,N}]$ and the largest CI is given by $[0.84p_{e,N}, 1.16p_{e,N}]$. So, the proposed kernel-based SEP estimator is highly reliable under the three types of channel models.

The performance achieved in terms of accuracy and reliability by the proposed kernel-based SEP estimator is at the cost of a certain sample size N_K , i.e., the amount of soft observations that

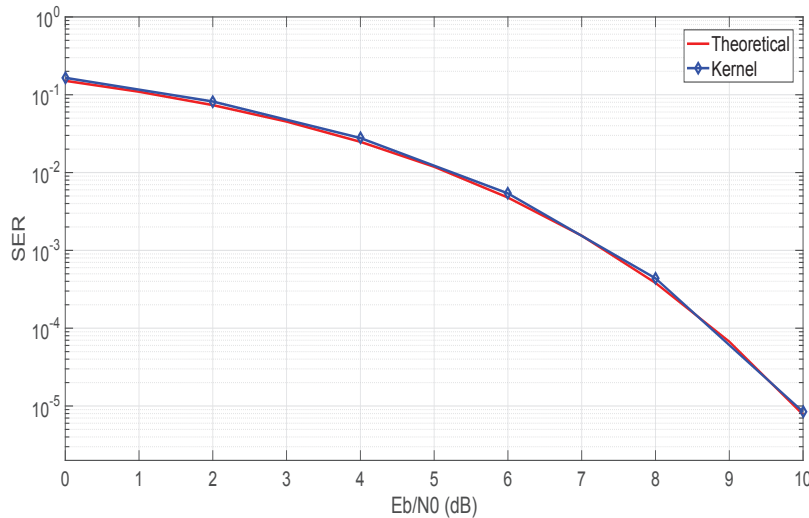


Figure 1: 4-QAM SEP estimates over the AWGN channel.

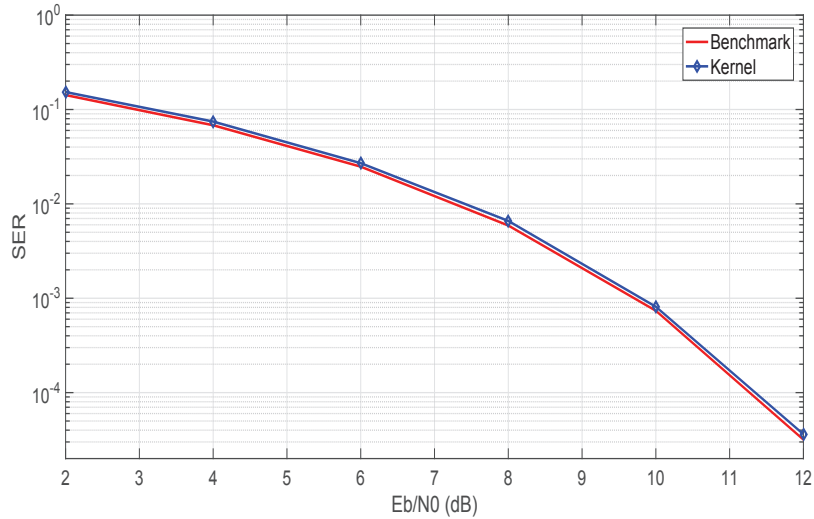


Figure 2: 4-QAM SEP estimates over the the frequency-selective channel.

were used for the estimation. In the fith columns of Table 1, Table 2 and Table 3, the different

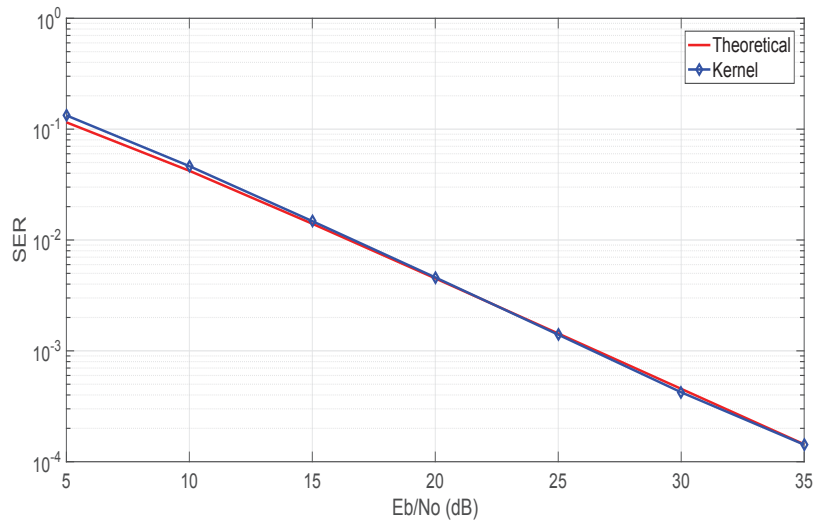


Figure 3: 4-QAM SEP estimates over the Rayleigh channel.

E_b/N_0 (dB)	$p_{e,N}$	Absolute bias	Two-sided CI	N_K	N_{mc}
00	1.51×10^{-1}	0.14×10^{-1}	$[0.99p_{e,N}, 1.01p_{e,N}]$	3.0×10^3	4.5×10^3
02	7.36×10^{-2}	0.83×10^{-2}	$[0.99p_{e,N}, 1.01p_{e,N}]$	6.0×10^3	9.0×10^3
04	2.48×10^{-2}	0.30×10^{-2}	$[0.99p_{e,N}, 1.01p_{e,N}]$	1.5×10^4	3.5×10^4
06	4.80×10^{-3}	0.60×10^{-3}	$[0.99p_{e,N}, 1.01p_{e,N}]$	3.5×10^4	5.5×10^4
08	3.82×10^{-4}	0.56×10^{-4}	$[0.97p_{e,N}, 1.03p_{e,N}]$	1.0×10^5	1.5×10^5
10	7.74×10^{-6}	0.67×10^{-6}	$[0.85p_{e,N}, 1.15p_{e,N}]$	2.0×10^5	2.3×10^5

Table 1: Numerical data characterising the SEP estimates over the AWGN channel.

sample sizes N_K that characterise the achieved performance are given. In the last columns of Table 1, Table 2 and Table 3, numerical data corresponding to the sample sizes N_{mc} that are required by the standard MC to achieve the SEP estimations with almost equal reliability and accuracy are also given. The values of N_{mc} have been determined by simulations. Compared to the sample sizes N_{mc} , the sample sizes N_K are smaller. This results in sample size savings making the proposed SEP estimator more efficient than the standard MC. However, we may wonder if the achieved sample size savings would be enough to declare the proposed estimator efficient indeed. To answer this query, let us analyse the efficiency of the estimation in terms of CPU time. Based on the numerical data regarding the SEP estimations over the frequency-selective Rayleigh fading

$E_b/N_0(dB)$	$p_{e,N}$	Absolute bias	Two-sided CI	N_K	N_{mc}
02	1.42×10^{-1}	0.11×10^{-1}	$[0.99p_{e,N}, 1.01p_{e,N}]$	5.0×10^3	9.0×10^3
04	6.81×10^{-2}	0.64×10^{-2}	$[0.99p_{e,N}, 1.01p_{e,N}]$	1.0×10^4	1.5×10^4
06	2.48×10^{-2}	0.22×10^{-2}	$[0.99p_{e,N}, 1.01p_{e,N}]$	3.0×10^4	4.0×10^4
08	5.90×10^{-3}	0.70×10^{-3}	$[0.99p_{e,N}, 1.01p_{e,N}]$	5.0×10^4	7.0×10^4
10	7.37×10^{-4}	0.76×10^{-4}	$[0.98p_{e,N}, 1.02p_{e,N}]$	1.0×10^5	1.2×10^5
12	3.18×10^{-5}	0.45×10^{-5}	$[0.90p_{e,N}, 1.10p_{e,N}]$	1.0×10^5	1.6×10^5

Table 2: Numerical data characterising the SEP estimates over the frequency-selective channel.

$E_b/N_0(dB)$	$p_{e,N}$	Absolute bias	Two-sided CI	N_K	N_{mc}
05	1.15×10^{-1}	0.18×10^{-1}	$[0.92p_{e,N}, 1.08p_{e,N}]$	3.0×10^4	1.0×10^4
10	4.21×10^{-2}	0.43×10^{-2}	$[0.90p_{e,N}, 1.10p_{e,N}]$	3.0×10^4	6.0×10^4
15	1.40×10^{-2}	0.08×10^{-2}	$[0.88p_{e,N}, 1.12p_{e,N}]$	3.0×10^4	6.0×10^4
20	4.50×10^{-3}	0.10×10^{-3}	$[0.87p_{e,N}, 1.13p_{e,N}]$	3.0×10^4	6.0×10^4
25	1.40×10^{-3}	0.00×10^{-3}	$[0.86p_{e,N}, 1.14p_{e,N}]$	3.0×10^4	7.0×10^4
30	4.54×10^{-4}	0.31×10^{-4}	$[0.84p_{e,N}, 1.16p_{e,N}]$	3.0×10^4	8.0×10^4
35	1.44×10^{-4}	0.01×10^{-4}	$[0.84p_{e,N}, 1.16p_{e,N}]$	6.0×10^4	1.3×10^5

Table 3: Numerical data characterising the SEP estimates over the Rayleigh channel.

channel, we observed gains of efficiency in terms of the computational cost. For instance, we noted for $E_b/N_0 = 30 dB$ (see the corresponding row in Table 3) that the proposed SEP estimator performed using a sample size $N_K = 3.0 \times 10^4$ and engendering a computational cost (i.e., the CPU time) of 2.0 s. In the same conditions of transmission and achieving the same accuracy and reliability performance, the standard MC method used a sample size $N_{mc} = 8.0 \times 10^4$ causing a higher CPU time equal to 4.89 s. A second illustration, based on the data of the last row of Table 3, reveals a CPU time of 3.64 s against 7.87 s for the standard MC method. CPU time savings are therefore achieved. These CPU time savings, although they seem small, may be of a great interest in green computing.

The asymptotic behaviour of the proposed kernel-based SEP estimator is illustrated in Table 4 for transmissions over the frequency-selective channel under two different E_b/N_0 values. We can see that the absolute bias and the CI become smaller as the sample size N_K increases.

$E_b/N_0(dB)$	N_K	Absolute bias	Two-sided CI
02	3,000	0.14×10^{-1}	$[0.989p_{e,N}, 1.011p_{e,N}]$
	4,000	0.12×10^{-1}	$[0.992p_{e,N}, 1.008p_{e,N}]$
	5,000	0.11×10^{-1}	$[0.993p_{e,N}, 1.007p_{e,N}]$
	6,000	0.10×10^{-1}	$[0.993p_{e,N}, 1.007p_{e,N}]$
12	5,000	2.35×10^{-5}	$[0.573p_{e,N}, 1.427p_{e,N}]$
	10,000	2.11×10^{-5}	$[0.601p_{e,N}, 1.399p_{e,N}]$
	50,000	0.86×10^{-5}	$[0.862p_{e,N}, 1.138p_{e,N}]$
	100,000	0.45×10^{-5}	$[0.903p_{e,N}, 1.097p_{e,N}]$

Table 4: Asymptotic behaviour of the proposed SEP estimator.

6. Conclusion

In this paper, we investigated the problem of efficient Symbol Error Probability (SEP) estimation for the transmission systems based on Quadrature Amplitude Modulation (QAM) schemes. We designed a Gaussian kernel-based SEP estimator that allows, using soft observations at the receiver-end, to compute the Symbol Error Rate of any digital communication system built over a QAM transceiver. We first established the formal expression of the SEP and presented the way it can be estimated using kernel density estimators. Then, we applied a two-dimensional kernel density estimators technique to obtain a convenient equation of the SEP estimate that can be computed by simulation. We used soft 4-QAM symbols sampled from the channel output and run simulations under three different types of transmission channels: the Additive White Gaussian Noise channel, a frequency-selective channel and a multipath Rayleigh fading channel. We reported simulation results of the kernel-based SEP estimates and analysed, using absolute bias and confidence interval, the performance of the estimator in terms of accuracy and reliability. For equivalent accuracy and reliability, we compared the proposed kernel-based SEP estimator to the standard Monte Carlo simulation technique and found that the proposed estimator is more efficient. We evaluated its efficiency on both levels of sample size and CPU time savings. The overall performance of the proposed kernel-based estimator was concluded highly accurate and reliable to the trade-off of an efficiency up to a factor two. The achieved efficiency of the kernel-based estimator can be of greater significance in some issues resolution that are better addressed by the green computing research area.

References

- [1] S. Benedetto, E. Biglieri, R. Daffara. *Modeling and performance evaluation of non linear satellite links-A volterra series approach*. IEEE Journal on Selected Areas in Communications, AES-15 (1979), 494-507.
- [2] K. Yao, L. B. Milstein. *The use of moment space bounds for evaluating the performance of a non linear digital communication system*. IEEE Transactions on Communications, 31 (1993), 677-683.
- [3] C. M. Jeruchim. *Techniques for estimating the bit error rate in the simulation of digital communication systems*. IEEE Journal on Selected Areas in Communications, 2 (1984), No. 1, 153-170.
- [4] K. Shanmugan, P. Balaban. *A Modified Monte-Carlo Simulation Technique for the Evaluation of Error Rate in Digital Communication Systems*. IEEE Transactions on Communications, 28 (1980), No. 11, 1916-1924.
- [5] S. B. Weinstein. *Theory and application of some classical and generalized asymptotic distributions of extreme values*. IEEE Transactions on Information Theory, 19 (1973), No. 2, 148-154.
- [6] S. B. Weinstein. *Estimation of small probabilities by linearization of the tail of a probability distribution function*. IEEE Transactions on Communication Technology, 19 (1971), No. 6, 1149-1155.
- [7] M. Rosenblatt. *Remarks on some non-parametric estimates of a density function*. The Annals of Mathematical Statistics, 27 (1956), No. 3, 832-837.
- [8] S. Saoudi, F. Ghorbel and A. Hillion. *Some statistical properties of the kernel-diffeomorphism estimator*. Applied Stochastic Models and Data Analysis Journal, 13 (1997), 39-58.
- [9] S. Saoudi, M. Troudi, F. Ghorbel. *An Iterative Soft Bit Error Rate Estimation of Any Digital Communication Systems Using a Nonparametric Probability Density Function*. EURASIP Journal on Wireless Communications and Networking, (2009), doi:10.1155/2009/512192.
- [10] S. Saoudi, T. Ait-Idir, Y. Mochida. *A Novel Non-Parametric Iterative Soft Bit Error Rate Estimation Technique for Digital Communications Systems*. IEEE International Conference on Communications (ICC), (2011), 1-6.
- [11] J. D. Laster, J. H. Reed, W. H. Tranter. *Bit Error Rate Estimation using Probability Density Function Estimators*. IEEE Transactions on Vehicular Technology, 51 (2003), No. 1, 260-267.
- [12] P. Poda, S. Saoudi, T. Chonavel, F. Guilloud, T. Tapsoba. *Kernel-based performance evaluation of coded QAM systems*. CARI 2016, Hammamet, Tunisie, (2016), 182-191.
- [13] P. Poda, T. Tapsoba, S. Saoudi, T. Chonavel, F. Guilloud. *A kernel-based soft BER estimator for coded QAM transmission systems*. IEEE International Symposium on Signal, Image, Video and Communications (ISIVC), (2016), 314-319.

- [14] P. Poda, S. Saoudi, T. Chonavel. *An efficient Kernel-Based Technique for QAM Symbol Error Probability Estimation*. IEEE Wireless Communications and Networking Conference Workshops (WCNCW), (2017), 1-6.
- [15] P. Poda, S. Saoudi. *A kernel-based QAM symbol error probability estimation Technique*. IEEE Vehicular Technology Conference (VTC-Fall), (2017), Toronto, Canada (accepted).
- [16] I. Kom, L. M. Hii. *Relation Between Bit and Symbol Error Probabilities for DPSK and FSK with Differential Phase Detection*. IEEE Transactions on Communications, 42 (1994), No. 10, 2778-2780.
- [17] Z. Z. Adriano, D. Ronaldo. *A review of kernel density estimation with application to econometrics*. International Econometric Review, 5 (2013), 20-42.
- [18] K. S. Shanmugan, A. M. Breipohl. *Random Signals: Detection, Estimation, and Data Analysis*. Wiley, New York, 1988.
- [19] M. Troudi, A. M. Alimi, S. Saoudi. *Fast plug-in method for parzen probability density estimator applied to genetic neutrality study*. International Conference on Computer as a Tool (EUROCON'07), (2007), 1034-1039.
- [20] J. G. Proakis, M. Salehi. *Digital Communications*. Mc Graw Hill, 5th edition, New York, 2008.
- [21] T. S. Rappaport. *Wireless Communications principles and practice*. New Jersey: Prentice Hall PTR, 1996.
- [22] J. R. Barry, E. A. Lee, D. G. Messerschmitt. *Digital Communication*. Kluwer Academic Publishers, 3rd edition, 2004.

Efficient Use of the Spectrum in Small Cell Deployments for 5G Wireless Communications Networks

Sandra LAGEN, Adrian AGUSTIN, and Josep VIDAL

Universitat Politècnica de Catalunya, Dept. Signal Theory and Communications, Signal Processing
and Communications Group, C/ Jordi Girona 1-3 08034 Barcelona (Spain)
Corresponding authors, E-mail: {sandra.lagen, adrian.agustin, josep.vidal}@upc.edu

Abstract. *Paired frequency division duplexing (FDD) bands are traditionally adopted at macro cells (MeNBs) but they tend to show inefficient occupancy of the uplink (UL) band due to the asymmetric traffic conditions and prevalence of downlink (DL)-centric applications. To improve spectrum utilization, one possibility is to allow time division duplexing (TDD) small cells (SeNBs) to operate in the underutilized FDD-UL spectrum. However, under an opportunistic access, TDD SeNBs might reuse the same resources as the FDD MeNB to receive in UL and, hence, strong interferences may appear. In this paper, we investigate advanced transmit coordination strategies to allow interference decoding and suppression at the MeNB such that the macro user signal can be decoded interference-free. We propose a novel technique to limit the maximum transmission rate of TDD SeNBs as a function of their distance to the MeNB in a way such that interference decoding and suppression is feasible. Simulation results show that sum-rate gains are obtained when the SeNB is close to the MeNB or when the SeNB transmits at high power (i.e. high interference conditions) as compared to a fully opportunistic access, while the proposed approach allows maintaining normal MeNB operation.*

Key words: flexible duplexing, paired FDD bands, asymmetric traffic conditions, interference decoding and suppression, transmit coordination.

1. Introduction

The almost universal adoption of advanced smartphones has produced a direct impact on the technical requirements of cellular networks, which have been compelled to improve spectral efficiency and spectrum utilization of wireless systems in order to satisfy the increased traffic demands generated by mobile users. The common technical solution adopted worldwide was the use of paired bands under frequency division duplexing (FDD) at macro cells (MeNB), which allocate the same amount of spectrum for both downlink (DL) and uplink (UL) communications. However, due to the overwhelming advent of data services, which are usually predominated by DL-centric applications [1] and impose large traffic asymmetries between DL and UL [2], the conventional paired FDD solution becomes highly spectrally inefficient.

One of the envisioned solutions to improve spectral efficiency and spectrum utilization is to densify the network with small cells (SeNBs), so that the spectrum can be spatially reused [3]. As FDD-based networks with a preassigned paired spectrum tend to have a large amount of unused resources in the FDD-UL band, such resources could be efficiently exploited if multiple time division duplexing (TDD) SeNBs are allowed to operate in the underutilized UL spectrum of an FDD MeNB [4]. Current 3GPP LTE standard and regulation do already hamper the use of these unused resources for DL transmission [5].

The FDD MeNB and TDD SeNBs can access the licensed FDD-UL bandwidth through different access methods: orthogonal or non-orthogonal. Under orthogonal access, MeNB and SeNBs are coordinated to use different time/frequency resources, hence avoiding co-channel interference but requiring of a tight coordination and a proper system configuration [6][7]. An overview of regulation, LTE standardization issues, and different technical solutions based on orthogonal access are provided in [4]. A simpler access is the non-orthogonal one, in which SeNBs are allowed to employ all the resources in the FDD-UL band and hence the MeNB and SeNBs might interfere each other, as shown in Figure 1. Here, we focus on the non-orthogonal access in the underutilized FDD-UL band.

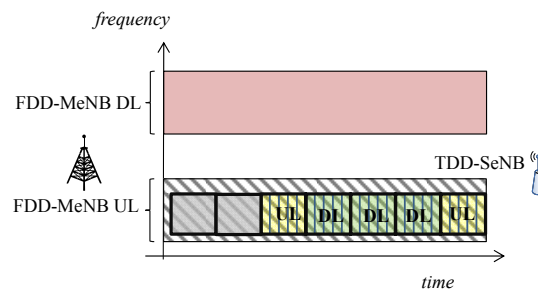


Figure 1. Non-orthogonal access between MeNB and SeNB in the licensed bandwidth for FDD-UL.

Under non-orthogonal access, the main impairment is the co-channel interference generated due to the simultaneous operation of the macro users (MUEs) and the transmissions in TDD mode of either the SeNB or its small users (SUEs). In particular, the most harmful interference situation appears when the SeNB transmits in DL because of the likely line-of-sight (LOS) condition between SeNB and MeNB, which generates DL-to-UL interference from the SeNB towards the MeNB that is receiving in UL. In this context, this paper investigates advanced coordinated strategies and interference mitigation techniques so as to deal with the predominant DL-to-UL interference when shared access in the FDD-UL band is attempted.

A well-known technique to deal with strong interference conditions is the interference decoding and suppression strategy, which has been extensively analyzed in literature and standardization bodies, see [8][9]. For example, 3GPP LTE investigated advanced receivers in the study item “Network-Assisted Interference Cancellation and Suppression (NAICS)” [8], in which all receivers belonging to the family of Interference Cancellation (IC) receivers are based on interference decoding and suppression. The key idea is that the receiver employs a non-linear receive filter to *decode* data symbols of the received interference and then *subtract* it from the received signal, and does so successively until decoding of the useful signal is done interference-free. Also, under dynamic TDD systems, 3GPP LTE analyzed through the study item “enhanced Interference Management and

Traffic Adaptation (eIMTA)” [9] the so-called Interference Suppressing Interference Mitigation strategy (ISIM), where interference decoding and suppression is considered for suppressing one or more dominant DL-to-UL interfering signals in a dynamic TDD system.

Decoding data symbols of the interferer can be performed provided that the interfering signal is received with an acceptable signal-to-interference-plus-noise ratio (SINR). On the other hand, for interference subtraction, perfect knowledge of the interfering channel is required. In this sense, all previous works ([8][9] and references therein) have dealt with the design and evaluation of the receiver capabilities to decode and suppress interference. Differently, in this paper, we will devise a coordinated transmission strategy that will allow a feasible implementation of interference decoding and subtraction.

We focus on the situation in which the FDD MeNB is receiving in UL and the TDD SeNB is transmitting in DL in the FDD-UL band to improve spectrum usage, as shown in Figure 2. In this scenario, interference decoding and suppression would ideally allow: *i*) decoding at the MeNB the data symbols transmitted by the interferer (i.e. the SeNB), *ii*) subtracting them from the received signal at the MeNB, and then *iii*) decoding the useful signal (received from the MUE) at the MeNB without interference. It is important to note that, thanks to the static positions of MeNB and SeNBs, the propagation channel between MeNB and SeNBs can be accurately estimated because of the long coherence time. This suggests that decoding of the data symbols sent by the SeNB is possible at the MeNB. However, not only channel estimation is required for interference decoding and suppression but also the SeNB should transmit at a rate that allows decoding of the interference at the MeNB. A key observation in this respect is that if the SeNB transmits at its maximum rate to serve its associated nearby user, usually this corresponds to a rate higher than the one that can be decoded at the MeNB due to the close SeNB-SUE distance. In this sense, we investigate procedures to limit the transmission rate at the SeNBs for DL transmissions in such a way that the data symbols sent by the SeNB can be properly decoded at the MeNB and, hence, efficient interference decoding and subtraction is permitted.

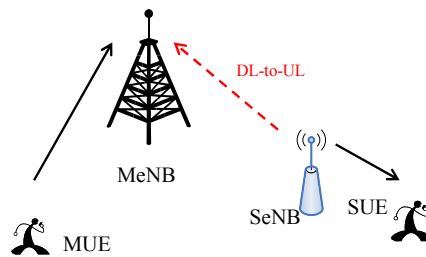


Figure 2. Target scenario composed of a MeNB receiving in UL and a SeNB transmitting in DL. Interference suppression will be implemented at the MeNB to decode and subtract the signal received from the SeNB.

The paper is organized as follows. Section 2 introduces the system model and the signal model. Then, in Section 3 we present the proposed transmit coordination strategy to allow decoding and subtraction of the interference at the MeNB. In Section 4, a statistical analysis is performed and analytical expressions for the maximum rate allowed at the SeNB and the attained rates on each link are derived. Section 5 includes the simulation results. Extension to the case of multiple TDD SeNBs accessing the FDD-UL band is analyzed in Section 6. Finally, conclusions are drawn in Section 7.

2. System model

Consider a paired FDD MeNB with underutilized spectrum in the FDD-UL band due to asymmetric traffic conditions. Assume TDD SeNBs are allowed to transmit/receive in the FDD-UL band to achieve better spectrum utilization through non-orthogonal access (i.e. there is no coordination in terms of the employed resources by the MeNB and the SeNBs, and so they may transmit on the same frequency/time resources simultaneously). We concentrate on a target scenario in which a SeNB transmits in DL and the MeNB receives in UL in the licensed FDD-UL band, as shown in Figure 2. Extension to the case of multiple TDD SeNBs is analyzed in Section 6.

In this setting, high DL-to-UL interference is generated from the SeNB towards the MeNB, see Figure 2. It is important to note two specific characteristics of the target scenario:

- without interference management, the signal from the MUE is received with a low SINR at the MeNB due to the strong DL-to-UL interference received from the SeNB with likely LOS condition.
- the signal from the SeNB is received in average with higher SINR at the SUE than at the MeNB due to the small SeNB-SUE distance.

The former can be addressed if the MeNB is able to decode and suppress the signal from the SeNB, such that the signal from the MUE could be decoded interference-free. The latter happens in all configurations even if LOS appears between SeNB and MeNB, because of the small distance between the SeNB and its SUE. Therefore, if we want to implement interference decoding and suppression at the MeNB (i.e. if we want the MeNB to decode the data symbols sent by the SeNB), then we need to redefine the SeNB transmit strategy so as to make possible decoding of the SeNB data symbols at the MeNB. Note that in case that the SeNB transmits at the highest rate towards its SUE, then data symbols sent by the SeNB may not be decoded by the MeNB because the achievable rate in the SeNB-to-MeNB link might be lower than the rate adopted at the SeNB for DL transmission. One way to allow the decoding is through the limitation of the transmission rate that is permitted at the SeNB to access the FDD-UL band. This is the main idea that will be proposed and analyzed in next sections. But, before proceeding, let us present the signal model.

The received signal at the MeNB and the SUE are, respectively:

$$\begin{aligned} y_{\text{MeNB}} &= g_{\text{MUE-MeNB}} \sqrt{P_{\text{MUE}}} x_{\text{MUE}} + g_{\text{SeNB-MeNB}} \sqrt{P_{\text{SeNB}}} x_{\text{SeNB}} + n_{\text{MeNB}} \\ y_{\text{SUE}} &= g_{\text{SeNB-SUE}} \sqrt{P_{\text{SeNB}}} x_{\text{SeNB}} + g_{\text{MUE-SUE}} \sqrt{P_{\text{MUE}}} x_{\text{MUE}} + n_{\text{SUE}} \end{aligned} \quad (1)$$

where x_{MUE} , x_{SeNB} are the signals transmitted by the MUE and the SeNB, respectively, P_{MUE} , P_{SeNB} denote the transmitted power at the MUE and the SeNB, respectively, g_{z-w} denotes the complex channel gain (including path-loss, shadowing, and fast fading) between the z -th terminal and the w -th terminal (where z, w refer to MeNB, SeNB, MUE, or SUE), and n_{MeNB} , n_{SUE} denote the complex circularly symmetric Gaussian noise components received at MeNB and SUE, respectively, with zero mean and variance σ^2 .

Under the scenario shown in Figure 2, the MeNB is interested in decoding x_{MUE} while the SUE is interested in decoding x_{SeNB} . In the SUE case, due to the close SeNB-SUE distance and low

probability of LOS between MUE and SUE (i.e. low probability of interference), the signal can be properly decoded in general. In contrast, the MeNB can be in trouble for decoding x_{MUE} because of the high levels of received interference due to likely LOS condition between SeNB and MeNB. Therefore, it is convenient to decode the SeNB signal at the MeNB and suppress it from the received signal.

In case that no interference decoding and suppression is performed at the MeNB, and under the assumption that interference is treated as Gaussian noise, the achievable rate of the MUE (for UL) and the SUE (for DL) are:

$$R_{\text{MUE-MeNB,int}} = \log_2(1 + \text{SINR}_{\text{MUE-MeNB}}), \quad \text{SINR}_{\text{MUE-MeNB}} = \frac{|g_{\text{MUE-MeNB}}|^2 P_{\text{MUE}}}{|g_{\text{SeNB-MeNB}}|^2 P_{\text{SeNB}} + \sigma^2} \quad (2)$$

$$R_{\text{SeNB-SUE}} = \log_2(1 + \text{SINR}_{\text{SeNB-SUE}}), \quad \text{SINR}_{\text{SeNB-SUE}} = \frac{|g_{\text{SeNB-SUE}}|^2 P_{\text{SeNB}}}{|g_{\text{MUE-SUE}}|^2 P_{\text{MUE}} + \sigma^2}$$

Assuming that the channel $g_{\text{SeNB-MeNB}}$ is perfectly acquired at the MeNB and interference decoding and suppression is performed at the MeNB, the processed received signal for MUE's signal decoding would be free of interference:

$$\tilde{y}_{\text{MeNB}} = y_{\text{MeNB}} - g_{\text{SeNB-MeNB}} \sqrt{P_{\text{SeNB}}} x_{\text{SeNB}} = g_{\text{MUE-MeNB}} \sqrt{P_{\text{MUE}}} x_{\text{MUE}} + n_{\text{MeNB}} \quad (3)$$

To allow decoding of the SeNB's data symbols at the MeNB (i.e. to allow obtaining the processed signal in (3)), our proposal is to limit the transmission rate at the SeNB. If said rate is not limited, then in most of the cases the MeNB would not be able to properly decode the SeNB signal if maximum rate is used at SeNB, and the achievable rates under interference conditions shown in (2) would be obtained.

4. Transmit Coordination Strategy

As previously mentioned, the signal from the SeNB is received in average with higher SINR at the SUE than at the MeNB. Therefore, our proposal is to limit the SeNB's transmission rate such that the SeNB signal can be decoded at the MeNB. This way, the MeNB could implement decoding and suppression of the interference, and then decode the MUE signal free of interference.

Let us denote by R_{SeNB} the transmission rate selected at the SeNB for DL transmission. On the other hand, the achievable rate for decoding the SeNB signal at the MeNB is:

$$R_{\text{SeNB-MeNB}} = \log_2(1 + \text{SINR}_{\text{SeNB-MeNB}}), \quad \text{SINR}_{\text{SeNB-MeNB}} = \frac{|g_{\text{SeNB-MeNB}}|^2 P_{\text{SeNB}}}{|g_{\text{MUE-MeNB}}|^2 P_{\text{MUE}} + \sigma^2} \quad (4)$$

In case that $R_{\text{SeNB}} \leq R_{\text{SeNB-MeNB}}$, then the MeNB is able to decode the signal received from the SeNB, subtract it from the received signal (as shown in (3)), and perform decoding of the MUE signal interference-free. Otherwise, if $R_{\text{SeNB}} > R_{\text{SeNB-MeNB}}$, then interference decoding is not possible.

Our proposal is to limit R_{SeNB} such that in a specific percentage of the situations (e.g. 90%) the SeNB signal can be decoded at the MeNB. Thus, in average, in 90% of the cases interference suppression is successful while in 10% of the cases the SeNB transmitted data symbols cannot be decoded at the MeNB.

By limiting the SeNB transmission rate in this way, we obtain the following:

- the MUE signal at the MeNB can be decoded interference-free in most of the cases (e.g. 90%), but
- the achievable rate of the SUE to access the licensed FDD-UL band is constrained.

Therefore, a clear trade-off arises. Depending on the MeNB-SeNB distance, LOS conditions, and transmit power of the SeNB, the limitation on the SeNB transmission rate might be either very strong or light (e.g. if the SeNB is far enough from the MeNB then R_{SeNB} would be very low, while if the SeNB is close to the MeNB then R_{SeNB} would be high and hence the MUE could be decoded interference-free while the rate of the SUE would be not much reduced as compared to its maximum rate).

In case of ideal decoding and $R_{\text{SeNB}} \leq R_{\text{SeNB-MeNB}}$, the achievable rate for the MUE (for UL) is interference-free:

$$R_{\text{MUE-MeNB,no-int}} = \log_2 (1 + \text{SNR}_{\text{MUE-MeNB}}), \quad \text{SNR}_{\text{MUE-MeNB}} = \frac{|g_{\text{MUE-MeNB}}|^2 P_{\text{MUE}}}{\sigma^2} \quad (5)$$

Note, however, that if $R_{\text{SeNB}} > R_{\text{SeNB-MeNB}}$ then the SeNB signal cannot be decoded at the MeNB and hence the rate for the MUE would be given by the one with interference shown in (2). On the other hand, the achievable rate for the SUE (for DL) is given by the minimum between the rate of the link and the rate imposed by the proposed transmission scheme:

$$R_{\text{SeNB-SUE}} = \min (R_{\text{SeNB}}, \log_2 (1 + \text{SINR}_{\text{SeNB-SUE}})) \quad (6)$$

being $\text{SINR}_{\text{SeNB-SUE}}$ shown in (2).

5. Statistical Analysis

In this section we characterize analytically the SeNB rate limitation expression (R_{SeNB}) and the rate expressions of the system as a function of the SeNB-MeNB distance ($d_{\text{SeNB-MeNB}}$) and the SeNB transmitted power (P_{SeNB}) for the proposed transmit coordination strategy that allows interference decoding and suppression presented in Section 4.

To perform the analysis, we adopt the following channel model: $|g_{z-w}|^2 = \frac{1}{kd_{z-w}^\alpha} |h_{z-w}|^2$, where h_{z-w} stands for the fast fading component in the z - w link and kd_{z-w}^α includes pathloss and shadowing losses (being them proportional to the distance between z -th and w -th terminals: d_{z-w}). For simplicity of the presentation, for the linear term k and the pathloss exponent α , we use subindex 1 to denote the SeNB-MeNB link, subindex 2 to refer to the MUE-MeNB link, subindex 3 for the SeNB-SUE link, and subindex 4 for the MUE-SUE link.

5.1. Rate limitation for SeNB

According to this channel characterization, we perform an analysis based on outage probabilities. The outage probability for interference decoding given that the SeNB transmits at a rate R_{SeNB} is:

$$P_{\text{out}} = \Pr\{R_{\text{SeNB-MeNB}} < R_{\text{SeNB}}\}, \quad R_{\text{SeNB-MeNB}} = \log_2 \left(1 + \frac{|h_{\text{SeNB-MeNB}}|^2 P_{\text{SeNB}} / (k_1 d_{\text{SeNB-MeNB}}^{\alpha_1})}{\sigma^2 + |h_{\text{MUE-MeNB}}|^2 P_{\text{MUE}} / (k_2 d_{\text{MUE-MeNB}}^{\alpha_2})} \right) \quad (7)$$

where $\Pr\{a < b\}$ denotes the probability of a being smaller than b .

We assume that the SeNB-to-MeNB channel parameters are known at the MeNB and that $|h_{\text{MUE-MeNB}}|^2 = \gamma$ is an exponential random variable with mean $\bar{\gamma} = E\{|h_{\text{MUE-MeNB}}|^2\}$, being $E\{\cdot\}$ the expectation operator. We also consider that UL power control is adopted at MUEs to transmit towards the MeNB (a typical assumption in 3GPP LTE), such that the ratio $c_2 = P_{\text{MUE}} / (k_2 d_{\text{MUE-MeNB}}^{\alpha_2})$ is fixed. This way, the outage probability in (7) is reduced to:

$$\begin{aligned} P_{\text{out}} &= \Pr \left\{ \log_2 \left(1 + \frac{(P_{\text{SeNB}} / d_{\text{SeNB-MeNB}}^{\alpha_1}) c_1}{\sigma^2 + c_2 \gamma} \right) < R_{\text{SeNB}} \right\} \\ &= \Pr \left\{ (P_{\text{SeNB}} / d_{\text{SeNB-MeNB}}^{\alpha_1}) c_1 - (2^{R_{\text{SeNB}}} - 1) \sigma^2 - (2^{R_{\text{SeNB}}} - 1) c_2 \gamma < 0 \right\} \end{aligned} \quad (8)$$

where $c_1 = |h_{\text{SeNB-MeNB}}|^2 / k_1$. By solving the inequality in (8) and using the fact that γ is an exponential random variable with mean $\bar{\gamma}$, we have:

$$P_{\text{out}} = \int_{\gamma_0}^{\infty} \frac{1}{\bar{\gamma}} e^{-x/\bar{\gamma}} dx = e^{-\gamma_0/\bar{\gamma}}, \quad \gamma_0 = \frac{(P_{\text{SeNB}} / d_{\text{SeNB-MeNB}}^{\alpha_1}) c_1 - (2^{R_{\text{SeNB}}} - 1) \sigma^2}{(2^{R_{\text{SeNB}}} - 1) c_2} \quad (9)$$

If we set an outage probability of P_ϵ , i.e. $P_{\text{out}} = e^{-\gamma_0/\bar{\gamma}} = P_\epsilon$ in (9), then we obtain:

$$\frac{(P_{\text{SeNB}} / d_{\text{SeNB-MeNB}}^{\alpha_1}) c_1 - (2^{R_{\text{SeNB}}} - 1) \sigma^2}{(2^{R_{\text{SeNB}}} - 1) c_2 \bar{\gamma}} = \ln(1/P_\epsilon) \quad (10)$$

Finally, by developing the expression in (10), we get the relation between the maximum rate allowed at the SeNB (R_{SeNB}) and its transmitted power (P_{SeNB}) and the distance to the MeNB ($d_{\text{SeNB-MeNB}}$):

$$R_{\text{SeNB}} = \log_2 \left(1 + \frac{(P_{\text{SeNB}} / d_{\text{SeNB-MeNB}}^{\alpha_1}) c_1}{\sigma^2 + \ln(1/P_\epsilon) c_2 \bar{\gamma}} \right) \quad (11)$$

We can observe in (11) that the rate limitation directly depends on the ratio $P_{\text{SeNB}} / d_{\text{SeNB-MeNB}}^{\alpha_1}$. Therefore, increasing the SeNB transmitted power P_{SeNB} increases the maximum rate allowed at the SeNB R_{SeNB} . On the other hand, increasing the MeNB-SeNB distance $d_{\text{SeNB-MeNB}}$ decreases the maximum rate allowed at the SeNB R_{SeNB} .

Remark 1: If UL power control is adopted at users, the rate limitation for SeNB transmission shown in (11), which guarantees a feasible successive interference decoding and suppression statistically, does not depend on the specific MUE that is scheduled at the MeNB because c_2 in (11) is fixed.

Remark 2: If UL power control is not adopted at users, then the derivation is valid for a rate limitation at the SeNB that depends on the MUE scheduling (i.e. on the specific MUE that is scheduled at the MeNB, since c_2 in (11) would vary with the MUE). Thus, a coordinated scheduling at MeNB and SeNB could be derived with the objective that, depending on the MUE that is scheduled at the MeNB, the SeNB transmits towards a SUE that meets the maximum allowed rate. Otherwise, if we want to make the rate limitation independent of the specific MUE that is scheduled, then we should average over the statistics of the pathloss values for different MUEs.

5.2. Characterization of the average rates

To perform an analytic characterization of the average rates, let us assume that MUE-MeNB, SeNB-SUE, and MUE-SUE fast fading link gains follow an exponential random variable with mean equal to $\bar{\gamma}$, i.e. $\bar{\gamma} = E\{|h_{\text{MUE-MeNB}}|^2\} = E\{|h_{\text{SeNB-SUE}}|^2\} = E\{|h_{\text{MUE-SUE}}|^2\}$. Also assume that SeNB-SUE, MUE-SUE, and MUE-MeNB distances are uniformly distributed random variables with a known mean: $E\{d_{\text{MUE-MeNB}}\} = d_2$, $E\{d_{\text{SeNB-SUE}}\} = d_3$, $E\{d_{\text{MUE-SUE}}\} = d_4$ (in meters). In the present analysis we compute the average rates of the users in the target scenario depicted in Figure 2 based on the average SINR received on each link. Two different strategies are compared:

- ‘INT’: interference situation of a fully opportunistic access, whereby interference is simply treated as Gaussian noise.
- ‘SIC’: transmit coordination strategy proposed in Section 4, in which a maximum rate is allowed at the SeNB and interference decoding and suppression is applied at MeNB.

Under ‘INT’ strategy, the average sum-rate is given by:

$$SR^{\text{int}} = R_{\text{MUE-MeNB}}^{\text{int}} + R_{\text{SeNB-SUE}}^{\text{int}} \begin{cases} R_{\text{MUE-MeNB}}^{\text{int}} = \log_2 \left(1 + E \left\{ \frac{|h_{\text{MUE-MeNB}}|^2 P_{\text{MUE}} / (k_2 d_{\text{MUE-MeNB}}^{\alpha_2})}{\sigma^2 + (P_{\text{SeNB}} / d_{\text{SeNB-MeNB}}^{\alpha_1}) c_1} \right\} \right) \\ R_{\text{SeNB-SUE}}^{\text{int}} = \log_2 \left(1 + E \left\{ \frac{|h_{\text{SeNB-SUE}}|^2 P_{\text{SeNB}} / (k_3 d_{\text{SeNB-SUE}}^{\alpha_3})}{\sigma^2 + |h_{\text{MUE-SUE}}|^2 P_{\text{MUE}} / (k_4 d_{\text{MUE-SUE}}^{\alpha_4})} \right\} \right) \end{cases} \quad (12)$$

By averaging the SINR over the different random variables (fast fading link gains and distances), the rates are thus given by:

$$\begin{aligned} R_{\text{MUE-MeNB}}^{\text{int}} &= \log_2 \left(1 + \frac{\bar{\gamma} P_{\text{MUE}} / (k_2 d_2^{\alpha_2})}{\sigma^2 + (P_{\text{SeNB}} / d_{\text{SeNB-MeNB}}^{\alpha_1}) c_1} \right) \\ R_{\text{SeNB-SUE}}^{\text{int}} &= \log_2 \left(1 + \frac{\bar{\gamma} P_{\text{SeNB}} / (k_3 d_3^{\alpha_3})}{\sigma^2 + \bar{\gamma} P_{\text{MUE}} / (k_4 d_4^{\alpha_4})} \right) \end{aligned} \quad (13)$$

Under ‘SIC’ strategy, the average sum-rate computed by averaging the SINR over the fast fading link gain and distance random variables is given by:

$$\begin{aligned}
 SR^{\text{sic}} &= R_{\text{MUE-MeNB}}^{\text{sic}} + R_{\text{SeNB-SUE}}^{\text{sic}} \\
 &\left\{ \begin{aligned}
 R_{\text{MUE-MeNB}}^{\text{sic}} &= (1 - P_\epsilon) \log_2 \left(1 + \frac{\bar{\gamma} P_{\text{MUE}} / (k_2 d_2^{\alpha_2})}{\sigma^2} \right) + P_\epsilon \log_2 \left(1 + \frac{\bar{\gamma} P_{\text{MUE}} / (k_2 d_2^{\alpha_2})}{\sigma^2 + (P_{\text{SeNB}} / d_{\text{SeNB-MeNB}}^{\alpha_1}) c_1} \right) \\
 R_{\text{SeNB-SUE}}^{\text{sic}} &= \min \left(\log_2 \left(1 + \frac{(P_{\text{SeNB}} / d_{\text{SeNB-MeNB}}^{\alpha_1}) c_1}{\sigma^2 + \ln(1/P_\epsilon) c_2 \bar{\gamma}} \right), \log_2 \left(1 + \frac{\bar{\gamma} P_{\text{SeNB}} / (k_3 d_3^{\alpha_3})}{\sigma^2 + \bar{\gamma} P_{\text{MUE}} / (k_4 d_4^{\alpha_4})} \right) \right)
 \end{aligned} \right. \quad (14)
 \end{aligned}$$

Note that the SeNB transmission rate has been limited in such a way that the MUE-MeNB transmission is interference-free with probability $(1 - P_\epsilon)$, while there is a probability of P_ϵ to receive interference from the SeNB at the MeNB. On the other hand, the rate for SeNB transmission is given by the minimum between the average rate on the SeNB-SUE link and the maximum rate imposed by the proposed coordinated transmission scheme.

Therefore, we are interested in comparing the average sum-rates under ‘INT’ and ‘SIC’ strategies as a function of the ratio $X = P_{\text{SeNB}} / d_{\text{SeNB-MeNB}}^{\alpha_1}$:

$$\begin{aligned}
 SR^{\text{int}}(X) &= \log_2 \left(1 + \frac{\bar{\gamma} P_{\text{MUE}} / (k_2 d_2^{\alpha_2})}{\sigma^2 + X c_1} \right) + \log_2 \left(1 + \frac{\bar{\gamma} P_{\text{SeNB}} / (k_3 d_3^{\alpha_3})}{\sigma^2 + \bar{\gamma} P_{\text{MUE}} / (k_4 d_4^{\alpha_4})} \right) \\
 SR^{\text{sic}}(X) &= (1 - P_\epsilon) \log_2 \left(1 + \frac{\bar{\gamma} P_{\text{MUE}} / (k_2 d_2^{\alpha_2})}{\sigma^2} \right) + P_\epsilon \log_2 \left(1 + \frac{\bar{\gamma} P_{\text{MUE}} / (k_2 d_2^{\alpha_2})}{\sigma^2 + X c_1} \right) \\
 &\quad + \min \left(\log_2 \left(1 + \frac{X c_1}{\sigma^2 + \ln(1/P_\epsilon) \bar{\gamma} P_{\text{MUE}} / (k_2 d_2^{\alpha_2})} \right), \log_2 \left(1 + \frac{\bar{\gamma} P_{\text{SeNB}} / (k_3 d_3^{\alpha_3})}{\sigma^2 + \bar{\gamma} P_{\text{MUE}} / (k_4 d_4^{\alpha_4})} \right) \right) \quad (15)
 \end{aligned}$$

It can be observed in (15) that:

- $SR^{\text{int}}(X)$ is a **decreasing** function of $X = P_{\text{SeNB}} / d_{\text{SeNB-MeNB}}^{\alpha_1}$, i.e. increasing the SeNB transmitted power or decreasing the SeNB-MeNB distance involves a reduction of the sum-rate due to the increased level of interference received at the MeNB.
- $SR^{\text{sic}}(X)$ is the sum of an increasing function (the SUE rate is) and a decreasing function (the MUE rate) with respect to $X = P_{\text{SeNB}} / d_{\text{SeNB-MeNB}}^{\alpha_1}$. However, the predominant term is the one of the SUE (the MUE-MeNB transmission would receive interference with probability P_ϵ , e.g. only in the 10% of the cases), such that in general $SR^{\text{sic}}(X)$ in (15) is an **increasing** function of $X = P_{\text{SeNB}} / d_{\text{SeNB-MeNB}}^{\alpha_1}$.

According to this, a threshold for $X = P_{\text{SeNB}} / d_{\text{SeNB-MeNB}}^{\alpha_1}$ on which ‘INT’ is better than ‘SIC’ in terms of average sum-rate can exist. Note, however, that the proposed coordinated strategy can not only outperform a fully opportunistic access in the FDD-UL band (i.e. ‘INT’ strategy) but also allows the MeNB to maintain its usual operation in the FDD-UL band (i.e. as it was the only one there) while the ‘INT’ strategy can be very detrimental for MeNB operation.

6. Simulation Results

In this section we present the simulation results. Section 6.1 evaluates the maximum rate allowed at SeNB for DL transmission according to the expression derived in Section 5.1. Section 6.2 compares the average sum-rate and per-user rate performances of ‘INT’ and ‘SIC’ strategies, based on the developed expressions in Section 5.2. We consider $\bar{\gamma} = 1$, $|h_{\text{SeNB-MeNB}}|^2 = 1$, $\alpha_1 = \{2, 2.5, 3\}$, $\alpha_2 = 3$, $\alpha_3 = 3.5$, $\alpha_4 = 4$, $k_1 = k_2 = k_3 = k_4 = (4\pi/\lambda)^2$, $\lambda = 3 \times 10^8 / 3.5 \times 10^9$ (i.e. 3.5 GHz frequency carrier), $\sigma^2 = 10^{N/10}$, $N = -174 + 10 \log_{10}(2 \times 10^6)$ (i.e. 2 MHz bandwidth and noise spectral density equal to -174 dBm/Hz), $E\{d_{\text{MUE-MeNB}}\} = d_2 = 150$ m, $E\{d_{\text{SeNB-SUE}}\} = d_3 = 20$ m, $E\{d_{\text{MUE-SUE}}\} = d_4 = 100$ m. The MeNB-SeNB distance ($d_{\text{SeNB-MeNB}}$) will be varied through simulations. We use $P_\varepsilon = 0.1$ (i.e. ‘SIC’ strategy is designed in such a way that in 90% of the cases the interference can be decoded at MeNB). Transmit power at MUE (P_{MUE}) equal to 23 dBm is used. For the transmit power at SeNB (P_{SeNB}) we adopt two values: 24 dBm and 30 dBm. A maximum modulation and coding scheme (MCS) is adopted according to LTE.

6.1. Maximum rate at SeNB

Figure 3 displays the maximum rate allowed at the SeNB by following the expression in (11) as a function of the MeNB-SeNB distance ($d_{\text{SeNB-MeNB}}$) for a SeNB transmitted power of 24 dBm (left-figure) and 30 dBm (right-figure). In both cases, different values of the pathloss exponent in the SeNB-MeNB link are displayed ($\alpha_1 = \{2, 2.5, 3\}$). It can be observed that the maximum rate decreases as the MeNB-SeNB distance ($d_{\text{SeNB-MeNB}}$) increases and as the path loss exponent in the SeNB-MeNB link (α_1) increases. Also, the maximum rate decreases as the SeNB transmitted power (P_{SeNB}) decreases. Let us remark that the expression in (11) has been derived for the simplified pathloss model that depends on the pathloss exponent. Nevertheless, the analysis could be properly extended for more sophisticated channel models.

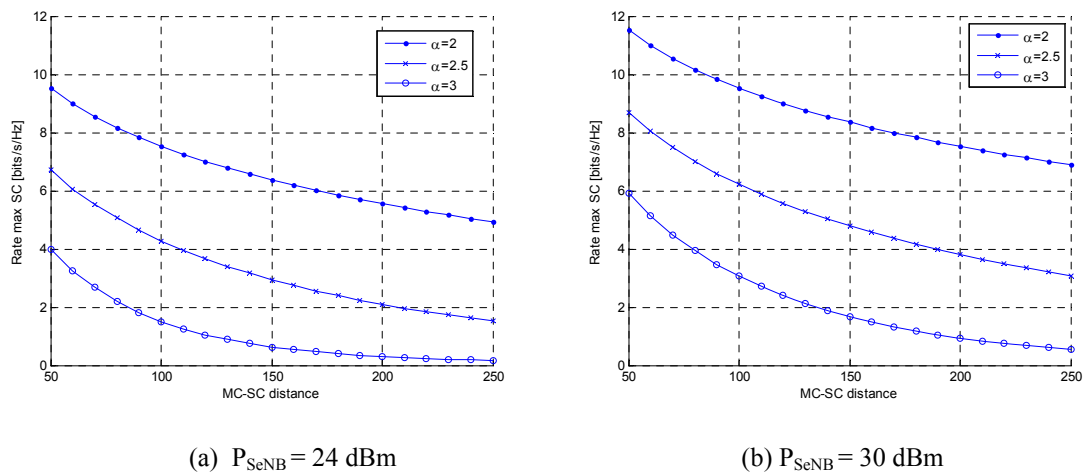


Figure 3. Maximum rate allowed at SeNB (in bits/s/Hz) vs. MeNB-SeNB distance ($d_{\text{SeNB-MeNB}}$, in m) for different values of the SeNB transmitted power (P_{SeNB}) and SeNB-MeNB path loss exponents (α_1).

6.2. Average sum-rate and per-user rate performance

Next figures show the average sum-rate of the users (left-figures) in the scenario shown in Figure 2 and the average rates for the SeNB-SUE link and the MeNB-MUE link, separately, (right-figures) under interference conditions ('INT' in figures, expression SR^{int} in (15)) and SIC assumption ('SIC' in figures, expression SR^{sic} in (15)) as a function of the MeNB-SeNB distance ($d_{SeNB-MeNB}$). Figure 4 displays the results for a SeNB transmitted power of 24dBm and Figure 5 for a SeNB transmitted power of 30dBm. Two different values of the pathloss exponent in the SeNB-MeNB link are considered: $\alpha_1 = \{2.5, 3\}$.

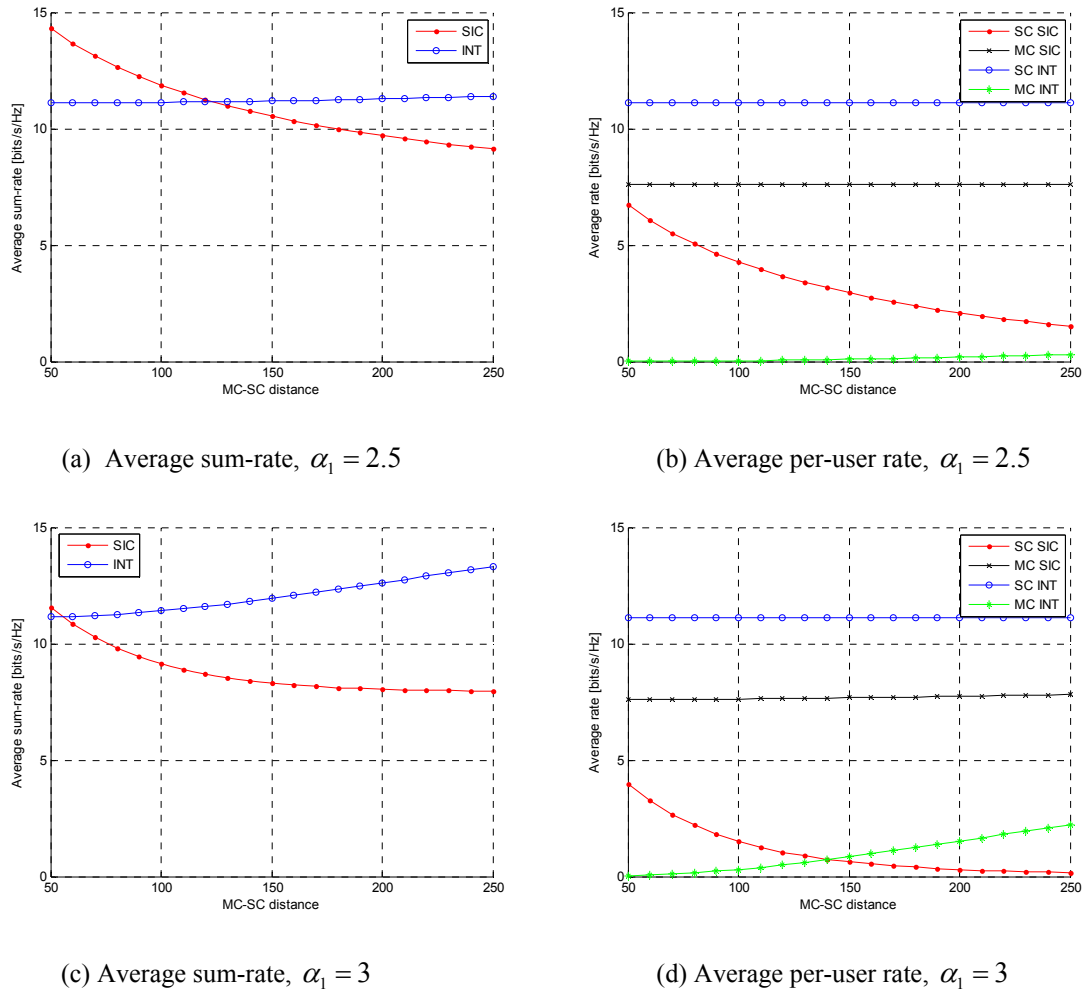


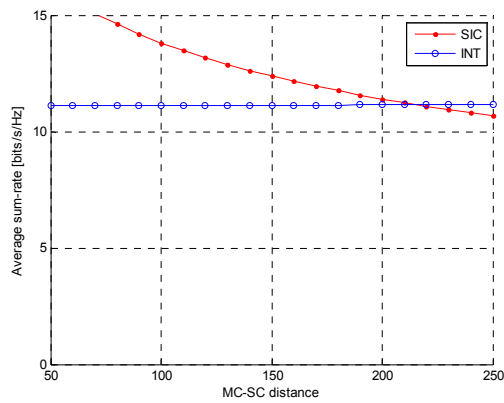
Figure 4. Average sum-rate and average per-user rate (in bits/s/Hz) vs. MeNB-SeNB distance ($d_{SeNB-MeNB}$, in m) under interference conditions ('INT') and the proposed SIC strategy ('SIC') for $P_{SeNB} = 24$ dBm and different SeNB-MeNB path loss exponents (α_1).

It can be observed that for low MeNB-SeNB distances, 'SIC' outperforms 'INT' in terms of average sum-rate while for large MeNB-SeNB distances the reverse situation is obtained. There is a threshold distance from which the best strategy in terms of average sum-rate changes. The threshold depends on the SeNB transmitted power and the propagation losses (which are modeled through the

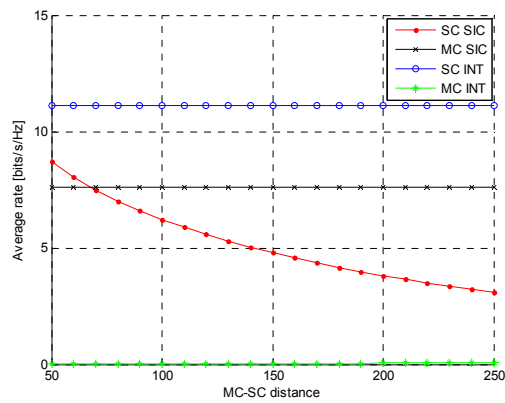
path loss exponent in the SeNB-MeNB link, α_1). In the scenario under consideration with simplified pathloss modelling, the thresholds for MeNB-SeNB distances correspond to:

- 124 m for $P_{\text{SeNB}} = 24$ dBm and $\alpha_1 = 2.5$ (see Figure 4.(a)),
- 55 m for $P_{\text{SeNB}} = 24$ dBm and $\alpha_1 = 3$ (see Figure 4.(c)),
- 215 m for $P_{\text{SeNB}} = 30$ dBm and $\alpha_1 = 2.5$ (see Figure 5.(a)),
- 88 m for $P_{\text{SeNB}} = 30$ dBm and $\alpha_1 = 3$ (see Figure 5.(c)).

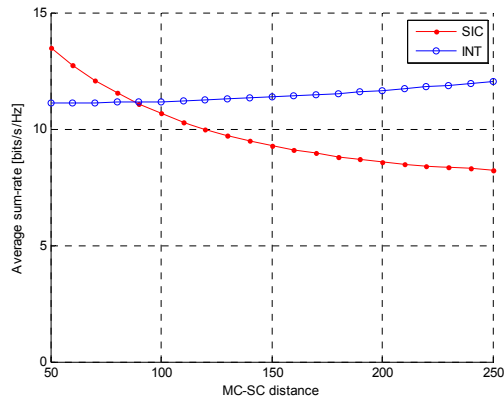
For fixed MeNB-SeNB propagation conditions, if the SeNB transmitted power is increased then the threshold distance is also increased (i.e. ‘SIC’ outperforms ‘INT’ in larger deployment distances). On the other hand, for a fixed SeNB transmitted power, if the MeNB-SeNB propagation conditions are improved (i.e. α_1 is reduced) then the threshold distance is also increased.



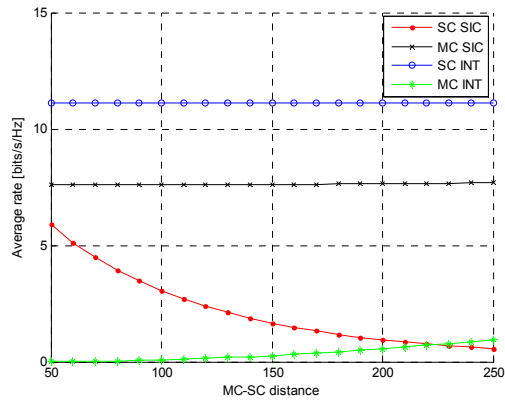
(a) Average sum-rate, $\alpha_1 = 2.5$



(b) Average per-user rate, $\alpha_1 = 2.5$



(c) Average sum-rate, $\alpha_1 = 3$



(d) Average per-user rate, $\alpha_1 = 3$

Figure 5. Average sum-rate and average per-user rate (in bits/s/Hz) vs. MeNB-SeNB distance ($d_{\text{SeNB-MeNB}}$, in m) under interference conditions (‘INT’) and the proposed SIC strategy (‘SIC’) for $P_{\text{SeNB}} = 30$ dBm and different SeNB-MeNB path loss exponents (α_1).

In Figure 4.(b)-(d) and Figure 5.(b)-(d) we can observe the behavior of the different average rates of the users. Under ‘SIC’ strategy, the average rate of the SeNB-SUE link is decreased with the

MeNB-SeNB distance due to the maximum rate allowed at SeNB (as it was shown in Figure 3) while the average rate of the MeNB-MUE link has a high value and a very low increase with respect to the MeNB-SeNB distance because the proposed ‘SIC’ strategy allows decoding the MUE signal interference-free at the MeNB in 90% of the cases (so, interference from the SeNB does not impact on the rate). Under ‘INT’ strategy, the average rate of the SeNB-SUE link does not vary with the MeNB-SeNB distance because the interference comes from the MUE, while the average rate of the MeNB-MUE link has a very low value and is increasing with the MeNB-SeNB distance because the farther the SeNB is the lower interference is received at MeNB.

It is very important to note that the average rate of the MeNB-MUE link is highly degraded due to interference, while the proposed transmit coordination approach for SIC implementation allows a very good rate at the MeNB-MUE link while constraining the SeNB-SUE average rate (i.e. the rate at which an SeNB that attempts to access the licensed FDD-UL band can transmit). Note that the average rate in the SeNB-SUE link corresponds to its maximum MCS under interference conditions for any MeNB-SeNB distance (and for that reason it does not vary with different SeNB transmitted power), because the SUE is placed close to the SeNB and the interference received from the MUE is very low and unlikely. Let us finally remark again that the expressions in (15) have been derived for the simplified pathloss model that depends on the pathloss exponent. However, the analysis could be extended for more sophisticated channel models.

6. Extension to multiple SeNBs

Assume that multiple TDD SeNBs are allowed to reuse the FDD-UL band where the MeNB operates in UL. Let us present, for simplicity, the case where we have just two SeNBs, as shown in Figure 6, although the concept can be easily extended to more than two SeNBs. To implement successive interference decoding and suppression at the MeNB it is convenient to have SeNBs at different distances (e.g. in Figure 6, SeNB 1 is closer to the MeNB than SeNB 2) such that the SeNBs can be ordered. Under this ordering, we will limit the transmission rate of the different SeNBs as follows.

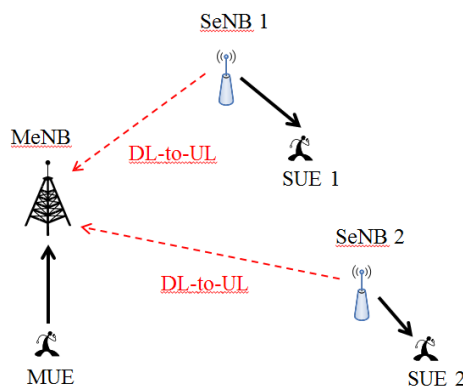


Figure 6. Extended scenario, composed of a MeNB receiving in UL and multiple SeNBs transmitting in DL. Interference suppression strategies are implemented at the MeNB to decode and suppress the signals received from the different SeNBs, successively.

First, SeNB 1 will need to be decoded with interference from SeNB 2 and MUE. So, we will limit its transmission rate such that in 90% of the cases the SeNB 1 signal can be decoded at the MeNB (assuming interference from SeNB 2 and MUE). Next, if decoding is successful, the signal from SeNB 1 will be subtracted from the received signal at the MeNB. Then, SeNB 2 signal will need to be decoded with interference from the MUE, such that we will limit its transmission rate in a way that in 90% of the cases the SeNB 2 signal can be decoded at the MeNB (assuming interference from MUE). Finally, if decoding is also successful, the signal from SeNB 2 will be subtracted from the received signal at the MeNB and the MUE signal could be decoded without interference.

This would be the way to proceed, i.e. by limiting the transmission rate of all SeNBs that cause major interference towards the MeNB, successively. Note that as more SeNBs coexist in the FDD UL band, more interference would be present to decode the signal from the first SeNB in the ordering. Thus, the rate of the closest SeNB would be the one more restricted. In this sense, the more SeNBs are allowed to transmit, the higher the sum-rate is increased but the lower are the individual transmission rates allowed at the SeNBs that are closer to the MeNB. Notice that this scenario is akin to the Multiple Access Channel [10].

7. Conclusion

In this paper we have proposed a coordinated strategy to limit the SeNB's transmission rate when the TDD SeNB is allowed to access the FDD-UL band of a MeNB. The rate limitation is made such that decoding of the SeNB data symbols at the MeNB is possible and hence it allows decoding of the useful MUE signal interference-free. The proposed approach constrains the rate of the SeNB but keeps nearly normal operation of the MeNB in the FDD-UL band. Extension to the case where multiple TDD SeNBs are deployed within the MeNB coverage areas is also analyzed.

The use of successive interference decoding and suppression at the MeNB through the limitation of the SeNB transmission rate for DL has been shown to provide gains in terms of average sum-rate as compared to a fully opportunistic access in two non-exclusive situations: when the SeNB is close to the MeNB and when the SeNB transmits at high power (i.e. high interference conditions). Otherwise, if the SeNB is far apart from the MeNB and uses low power, the average sum-rate under interference conditions without considering interference decoding and suppression provides a larger average sum-rate gain; however, the individual average rates of the MUEs are still degraded due to interference and normal MeNB operation is not maintained. This is resolved with the proposed strategy.

Acknowledgements

This work has been supported by Huawei Technologies Co. Ltd.

References

- [1] Qualcomm: Wireless broadband future and challenges, Oct. 2010.
- [2] DIGITALEUROPE: Call For Timely Harmonisation of the 1452-1492MHz and 2300-2400MHz Bands to Support Delivery of EU Radio Spectrum Policy Programme Objectives, Brussels, Feb. 2012.
- [3] N. Bhushan *et al.*, "Network densification: the dominant theme for wireless evolution into 5G," *IEEE Commun. Mag.*, vol. 52, pp. 82–89, Feb. 2014.
- [4] A. Agustin *et al.*, "Efficient use of paired spectrum bands through TDD small cell deployments", accepted for publication at *IEEE Commun. Mag.*, May 2017. Draft version available at <https://arxiv.org/abs/1612.02175>
- [5] 3GPP TR 36.882, "Study on regulatory aspects for flexible duplex for EUTRAN", Release 13, Sep. 2015.
- [6] 3GPP R1-134295, "FDD-TDD CA/Dual Connectivity solution exploiting traffic asymmetry in duplex-neutral bands", Oct. 2013.
- [7] S. Lagen *et al.*, "Long-term provisioning of radio resources based on their utilization in dense OFDMA networks", *IEEE Int. Symp. on Personal, Indoor and Mobile Radio Communications.*, Valencia (Spain), Sep. 2016.
- [8] 3GPP TR 36.866, "Study on Network-Assisted Interference Cancellation and Suppression (NAIC) for LTE", v12.0.1, Mar. 2014
- [9] 3GPP TR 36.828, "Further enhancements to LTE Time Division Duplex (TDD) for Downlink-Uplink (DL-UL) interference management and traffic adaptation", v11.0.0, Jun. 2012.
- [10] D. Tse, P. Viswanath, *Fundamentals of Wireless Communications*, Cambridge University Press, 2005

The Hassan mosque at the digital era

Farouk ACHAKIR^{1,4}, Marc Pierrot DESEILLIGNY³, Sanaa EL FKIH², Mina EL MGHARI⁴
Mohamed ETTARID⁵, El Mustapha MOUADDIB^{1,7} and Amina RADGUI⁶

¹ UPJV, Laboratoire MIS, Amiens - France

² ENSIAS, Rabat - Maroc

³ ENSG, Marne la Vallée - France

⁴ Université Mohammed V de Rabat - Maroc

⁵ IAV Hassan II, Rabat - Maroc

⁶ INPT, Rabat - Maroc

⁷ Corresponding author, E-mail : mouaddib@u-picardie.fr

Abstract.

About ten years ago, the double behest of late Driss Aboutajdine and El Mustapha Mouaddib permitted setting up research partnership on the use of image processing and cultural heritage. In 2015, despite his workload, Professor Driss Aboutajdine has put all his energy so a common complementary action could take place and occur, convening hence the numerical sciences, precisely 3D techniques, serving cultural heritage. This action went on to give birth to Athar-3D project, with the ambition to resolve questions pertaining to 3D modeling and computer vision having along a positive impact on cultural and architectural heritage perception. The research we carried out in this framework aims to the digitizing of Hassan Mosque, its reconstitution and the achievement of mechanism and application to heighten awareness and to better know and communicate about cultural heritage matter. To our knowledge, this is the first work of its kind and with this scientific extent on cultural and architectural heritage in Morocco. Moreover, finding an extension of academic research in the dissemination, the bringing back and mediation on this monument that stands for a symbol and emblem of Morocco's capital, is a direct valorization of research work performed in Moroccan research laboratories. This paper presents representative results of the whole project, including its historical and arts history, especially on Rabat Hassan Mosque. We are providing, for the first time, results that make possible 3D display of what Hassan Mosque might look like. This model with the vocation to be a scientific support and medium and to which we attempted to bring all the necessary rigor. This will serve the scientific study of the monument, the popularization and awareness raising with respect to cultural heritage matters in general and Hassan Mosque in particular.

We hope, therefore, to remain faithful to one of the wishes of Professor Driss Aboutajdine, which is to ensure that scientific research directly impact the society.

Key words : Hassan mosque, 3D modeling, reconstruction, digital heritage.

1. Digital Heritage issues

Architectural cultural heritage includes all evidence of human creativity and expression from the past. It is considered as a bridge between the past and the future. Exactly for this reason it is very important to preserve it. Besides Architectural cultural heritage contributes to the reinforcement and promotion of tourism and thus to economic development. In fact, this heritage is an important asset for the development and promotion of cultural tourism ; but it is also the witness of civilization over time. Morocco has a rich and diversified architectural and urban heritage, including buildings of different ages and architectural styles. In addition, it has an archaeological heritage of no less importance, made up of traces of ancient cultures and ancient civilizations several thousand years old ; a heritage to be proud of. The valorization of this history involves the preservation of this heritage through its inventory, its restoration and its conservation. These days, one way to achieve these objectives is a digitalization. Indeed, digital transformation is now a very interesting paradigm that complements and renews traditional means of safeguarding and mediation. The digitization techniques we have at present enable us to perpetuate the architectural cultural heritage to infinity in virtual form. Thus, 3D modeling makes restitutions, backup, reconstructions and studies possible either for better restoration or simply in order to better understand and thus better explain. See for examples works done in research program E-Cathedrale ([1]) and in [2]. During the last decade, automatic 3D modeling has made a signification progress thanks to, on the one hand, the emergence of a wide range of high performance laser scanners and affordable cost, on the other hand, the "go back" to photogrammetry which, thanks to algorithmic advances (Sift, Semi Global Matching ...) and the explosion of digital photography, has become a reliable and automatic modeling method in many contexts. In the aim to preserve the Moroccan architectural cultural heritage we proposed a research project called "Athar-3D project" (for 3D historical trace/footprint). This project is a marriage between 3D digital culture and architectural heritage. It meets both the needs of the general public for the varied uses of discovery and knowledge of heritage, as well as the demands of professionals and researchers for uses such as knowledge and scientific research, education and tourism. The 3D architectural heritage modeling has many challenges : the diversity of surfaces and objects requires the use of different forms for digitization, management of data heterogeneity, data size, scale and accessibility for digitization. In the effort to face these challenges, our contributions can be summarized as follows : study of a system for digitizing difficult-to-access objects and surfaces using a catadioptric approach for dense stereo vision, study of the fusion of laser scanners data and photogrammetry 3D point clouds, digitization of the Hassan mosque and multidisciplinary study on the contributions of the 3D model to the study of the Hassan mosque in Rabat. The Athar-3D project is supported by a bilateral Franco-Moroccan scientific cooperation program that is the Hubert Curien Partnership (PHC)¹ "Toubkal". It is carried out jointly by the Laboratory of Research in Computer Science and Telecommunications (LRIT- Laboratoire de Recherche en Informatique et Télécommunications) on the Moroccan side, and the Laboratory of Modeling, Information and Systems (MIS - Modélisation, Information et Systèmes) on the French side. In addition, several experts from the National Institute of Posts and Telecommunications (INPT), the Higher National School of Computer Science and Systems Analysis (ENSIAS-Mohammed V University in Rabat), and the Agronomic and Veterinary Institute Hassan II (IAV Hassan II), have been involved in this research project to validate the scientific part or the historical part. In addition, Ms. Mina El Mghari, art historian and professor at Mohammed V University in Rabat, is associated with the project to bring the skills of history and art history to the

1. <https://www.phc-france-maghreb.org/>

project. In this article, we try to present the preliminary results of this multidisciplinary collaboration which completes and renews some knowledge about the Hassan mosque. Hence, we will present the tools of digitization, the results obtained and the reflections resulting from the interactions between the digital model and the history of art. We also hope that this work, which is only at the beginning, will increase the interest for the Hassan mosque in particular and for the architectural heritage in general.

2. Digitization and reconstruction : background and tools

The need of professionals for 3D representation techniques as valuable source of detailed information has made of photogrammetry and lasergrammetry two attractive techniques. Regarding architectural applications, although lasergrammetry may seem to offer a better compromise between accuracy, speed of data acquisition, photogrammetry presents in many cases an interesting alternative to laser scanning surveys especially for outdoor modeling when it can be combined with UAV.

2.1. Digitization by photogrammetry

In the past, photogrammetry was based on sophisticated optical-mechanical equipment that limited its use due the high cost of this equipment and the need for well-trained personnel. The technological advances that affected photogrammetry lately and the bringing closer to computer vision have increased the interest and the use of photogrammetry in a variety of domains for automatic 3D modeling from multi-station photos. Nowadays, both the acquisition of photos and their processing are much flexible and within the reach of non-photogrammetrists provided the correct procedures are followed. Although the quality of the image is crucial, simple on the self-cameras can be used in either modes : static mode (terrestrial stations) or dynamic mode (van, uav,).

Once the photos are acquired, the general processing workflow goes through 3 sequential steps : first, the key points (or point of interest) are detected on overlapping photos having common coverage of the scene, second the relative orientation and bundle adjustment are done simultaneously and the last step is the generation of a dense points cloud by automatic correlation. Concerning the detection of key points or points of interest, many algorithms were developed in photogrammetry and computer vision, starting by a research done Hans Moravec back in 1981 and improved by others (Harris, Schmidt, Mohr, Forstner). The mostly used today in many software is the concept of Scale Invariant Feature Transform (SIFT) developed by Lowe. The concept transforms an image into a large collection of feature vectors, each of which is invariant to image translation, scaling, and rotation, partially invariant to illumination changes. SIFT operates in two main steps : a first algorithm detects the points of interest and a second algorithm is used for the matching.

Approaches using SFM (Structure from Motion) method, can simultaneously determine camera calibration, and camera position and orientation relative to the photographed object, for each photo. This is done by iteratively refining the intersection between bundles corresponding to homologous point. A 3D model of high level of details is then constructed by densifying the previous point cloud. The reconstructed 3D models can be rendered with realistic texture. One can also mesh the point cloud for subsequent advanced modeling and manipulation. Other products such orthophotos, vectors representing different structures of the object may be generated equally in an easy manner.

The process to produce this 3D model by Computer Vision community is now very well known. One can find easily toolboxes and software to realize automatically all needed

processing to produce these models. In our case, we used MicMac²[9] which is a free software produced by the IGN (partner of the consortium of Athar-3D project).

2.2. Digitization by laser scanner

With the increase of public awareness for the preservation of cultural heritage, the need is becoming important for new possibilities and ways to survey and document monuments and architectural and archeological sites for the analysis, modeling, reconstruction and communication on cultural heritage. Photogrammetry, close range mainly, has, for a long time, being used to provide accurate 2D and 3D data through the processing of stereo photos.

Late advances in the electronic domain and the emerging of laser scanning technology have opened new possibilities for professionals in charge of architectural documentation using laser. Hence, terrestrial laser scanner are nowadays widely used as they proved to be a valuable technology for the surveying of complex surfaces in a lesser time, accurately and with less effort.

In laser scanners, a laser beam is emitted from a laser light source and used to scan the surface of objects of interest. The laser beams has the ability to be oriented into varying directions by a system of mirrors combined with an instrument rotation.

Data acquired by the scanners consist in either Cartesian (XYZ) or polar coordinates (vertical and horizontal angle) augmented with information on the intensity (reflectance) of the received signal.

The data describing the detected 3D point could in space, can be visualized in 2D-image. In order to generate a 3D model of the object scanned, the scanner is generally placed in different stations in order to cover the entire object. The individual point clouds acquired from these stations should be registered in order to merge them to constitute the entire 3D model either in a local or global coordinate system. The software based on targets usually accomplishes this registration automatically. These targets are placed before scanning and shared by the clouds; in order the software can recognize them automatically later.

The quality of the cloud will depend on the accuracy of range determination, the size of the spot and the resolution and angular accuracy of the scanner. A camera may capture along with the scan photos to be used for the texturing of the 3D model when needed. But, the quality could be improved by using others images [3].

2.3. 3D modeling process

We will focus on Blender, but this process can be achieved using any other 3D creation software. Blender is a professional free and open-source 3D computer graphics software proposed to create 3D visualizations such as images, videos, and real-time interactive video games. The advantage of the 3D software like Blender is that it can be used in all stages of any architecture project. Blender is not the fastest tool in architecture but it is flexible when creating custom 3D shapes. The 3D reconstruction of any object of the mosque with Blender requires to identify the shape of the object, in the images of the book, and to measure the right dimensions on the plans. Blender tools allow manipulating simple geometrical shapes (circle, cylinder, sphere, ...) and to modify them according to the information provided by the images of the book and the plans. Blender's features include 3D modeling, UV unwrapping, texturing, sculpting and animating. Blender Modifiers are tools of 3D modeling that allow automatic operations that affect an object in a non-destructive way. They work by changing how an object is displayed and rendered, but not the geometry which remains stored in

2. <http://micmac.ensg.eu/>

computer memory. The Modifier Stack is used in case where several modifiers are added to a single object.

The process of creation of 3D model of each object in Blender is unique. However, many components of the mosque, such as arches, require the same steps during their creation. To illustrate this we give the example of the arches modeling. The general process of modeling arches is a Blender Modifier Stack. The four steps of this process (Fig. 1) are states of the arch during its creation and the links between them are Blender modifiers operations. The first step of the process is to create the 2D shape of the arch from its image. The second step is to generate a 3D object with the extrude tool and then correct it with Blender modifiers : Recalculate, Smooth and EdgeSplit to get the final 3D shape of the arch at the last step of the process.

The 3D Textured Mesh reconstruction from point cloud [5] is a process based on surface

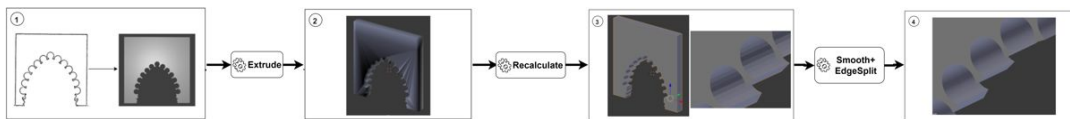


FIGURE 1 – General modeling process for Arches of Hassan mosque.

reconstruction algorithm that allows creating a 3D model from a point cloud. The importance of this method is to extract specifics elements of the point cloud like the pillars and then use them in the 3D reconstruction of the mosque. The algorithm described in [4] allows creating surface from oriented point sets.

The mesh is imported into Blender in PLY format (Polygon File format) and duplicated with Array modifier. Blender Cycle Render engine is used to detect the colors of the mesh vertices and to render the scene.

3. Toward a digital model of Hassan mosque

Our aim goal is to propose a 3D model of this mosque. We will proceed in two steps. The first one consists to digitize the existing part of this monument. This partial model will be used to have accurate measurements, textures and will serve as a digital copy of the existing part of the mosque. In the second step, we will complete the model by using the technics presented in section 3.2 and the reconstitution proposed in [7].

3.1. Hassan mosque

Hassan Mosque (Fig. 2) is an exceptional monument of Rabat city, which was built on a princely order. This huge project is the witness of a Moroccan architectural art that never ceased to evolve along the ruling of Almohade dynasty (1147-1269). This fine architectural grouping is an evidence of talented city planners, engineers, architects and great visual artists of Almohade epoch. Hassan Mosque is laying his vestiges within an area of the city called after him situated in the North East par of Rabat city. The monument is at Mohamed V Musoleum's feet, another masterly and modern architectural grouping. The Mosque was admittedly founded by the caliph Abu Yusuf Ya'qub Al-Mansour (1184-1199) in 599/1196 ; however, historical and archeological signs of evidence bring the monument to the father of Al Mansour Abu Yacoub Youssef. As for Rabat (Ribat Al Fath), the construction of

Hassan Mosque is the outcome of the dynasty policy or Jihad (holy war). In fact, the Jihad was the main reason behind Almohades establishing new Ribat cities. Rabat city is one of the major examples in this respect. Rabat City was conceived in Alexandria's image and endowed with Hassan Mosque, the tower of which dominates maritime entrance from the top of its 86 meters height. Many historical and archeological researches were devoted to Hassan Mosque vestiges. Since the beginning of the last century, amateurs and professionals were attracted by the site. In fact, the first surveys were launched in 1902. These were followed by series of excavations and prospecting, in 1913-1914 (Dieulafoy) [6] and 1933-1934 (Jules Borely). Investigations and topographic surveys, spread up to the foundations, undertaken by Historical Monuments Inspection in 1934-1944 (under the direction of H. Terrasse) revealed that the construction work was interrupted in 1199 following Al Mansour death. The different studies were crowned in 1949 by the work of Jacques Caillé and Jean Hainault [7]. Fig. 2 shows old and recent photographie of the esplanade. Fig. 3 shows a plan of global mosque as proposed by [7]. In red color, we added the actual remains of the esplanade.



FIGURE 2 – Photos of the Hassan Mosque. (a) Old photo (before restoration)(<https://www.delcampe.net/>). (b) Recent photo (2017).

3.2. Results of digitization

We realized the digitization of the esplanade Hassan in june 2015 (from june 8 to 12) by using lasergrammetry and photogrammetry. Unfortunately, at the same time, the tower was under renovation and the scaffolding obstructed its digitization. Therefore, it was not possible to scan the tower accurately (as we can see in the results sections) neither outside nor inside. The lasergrammetry was done with Leica C10 scanner³. We made 25 scans on the entire esplanade to cover all the columns. Fig. 4 shows captions from the 3D model. Fig. 5 shows some results from the photogrammetry, with camera poses. Red color is the frontal side of the camera when the green color mention the rest of the camera. The results of the photogrammetry have used for the texture of pillar, wall and the outside of walls.

These 3D models can serve for measurements, accurate plans, extraction of exact shapes and also as a didactic support to explain the history of the architecture of this mosque.

3. by help of GLOBETUDES Sarl company.

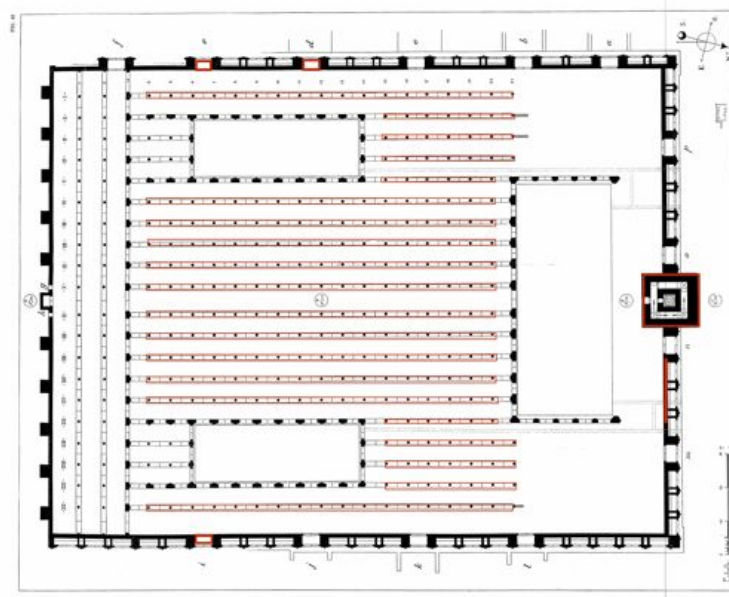


FIGURE 3 – Comparison between plan designed in [7] and the actual state on the esplanade. Red color indicates the common parts.

3.3. 3D reconstruction

In order to achieve the 3D reconstruction, we analyzed plans and descriptions of the mosque presented in [7] which is the most complete and up-to-date document written about this mosque. Fig. 6 shows two examples. These documents allowed us to realize a 3D model representing the missing parts of the Hassan mosque in Rabat.

The 3D digitization methods presented in Sec. 2.1 and 2.2, have been used to obtain the exact geometry, texture and color for the existing parts of the mosque. For the inexistent parts (arches and tiles), we have used historical sources, archives and archaeological excavations [7]. In the next we will give the results of the 3D reconstruction of five parts of the mosque.

- **Pillar model** : There are two types of pillar : the smallest pillar is used in the oratory hall except for the extreme aisles where the second type is used. We used the sizes given by the lasergrammetry. The texture has been obtained by the photogrammetry 3D model (Fig. 5) because the quality of images given by the internal camera of the scanner is not sufficient.
- **Arches model** : Many are smooth arches, which divide the aisles of the mosque between them and unite the oratory hall to the lateral gallery. However, there are also three kinds of lobed arches : arches with equal lobes, trefoil lobes or stalactites which emphasizes the importance of the central and extreme aisles. Fig. 7(a) shows

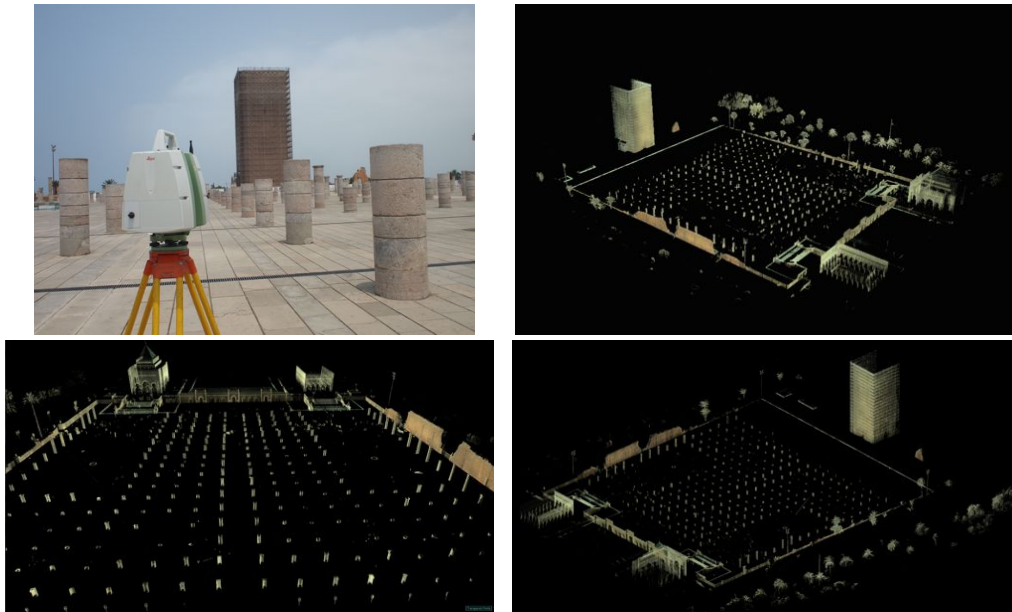


FIGURE 4 – View of the esplanade with the used scanner and captions from the 3D model got by lasergrammetry.

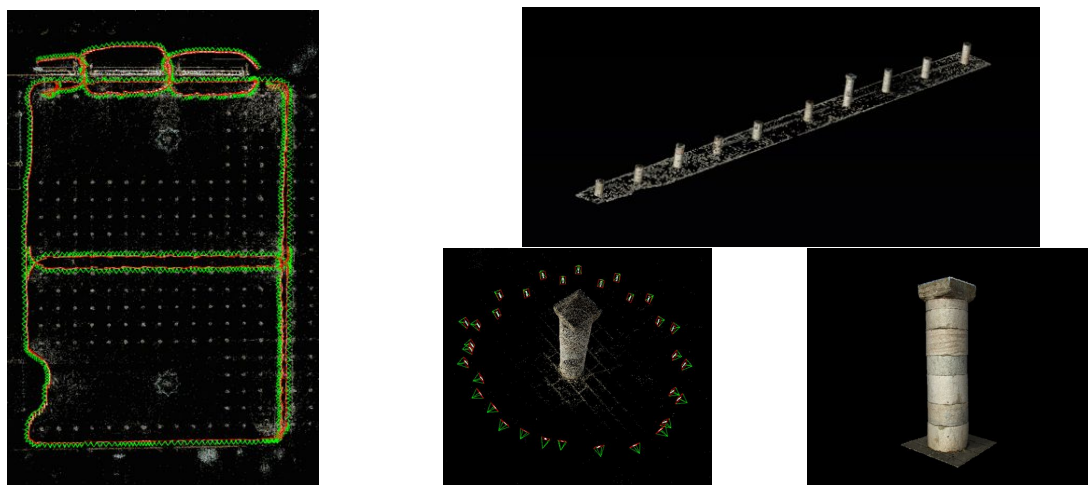


FIGURE 5 – (a) Global model and camera poses (green and red for frontal face), (b) Pillar and camera poses, (c) Dense 3D model for this pillar, (d) Row of pillars.

the restitution of the arches as they are on the plans of the mosque and Fig. 7(b,c,d) illustrates results of 3D reconstruction of all the existing arches in the mosque.

- **Outer wall** : The outer wall of the mosque is built by several basic elements that are modeled individually according to the dimensions expressed on the plans. The reconstruction process of the outer wall is composed of three steps that are :
 - Modeling the general form of the outer wall which surrounds the mosque. This step requires modeling stairs and all arches that represent the entries of the mosque.
 - Adding the decorative elements to the wall. There are two types of decorative elements on the plans : tiles and geometric form that are found above the wall and the minaret as well.
 - Adding texture to the wall. This texture is created after 3D mesh reconstruction process of the cloud of the wall. The textured mesh of the wall is then added to the 3D model of the second phase to obtain the final model of the outer wall.
 The same process was applied to the whole wall and the final result is shows in the Fig. 9.
- **Tile model** : The 3D modeling of the tile is based essentially on a single image given by [7] (see Fig. 10). The 3D model of tile is quite simple, but it is necessary to cover all the roofs and the outer wall of the mosque with thousands of tiles. This increase the rendering time of the final 3D model of the mosque. In order to reduce the amount of rendering time, we made sure we had as few vertices as possible on the tile model. In addition, we used the Blender Decimate modifier to decrement the number of vertices in tile model shown in Fig. 10.
- **Roof model** : The roof is composed by two types of elements : the small element covers the simple aisles and the larger one covers the central and extreme aisles of the mosque. The 3D reconstruction of the roof is achieved manually by duplicating the two above elements. The Fig. 10 shows the restitution of the roof.

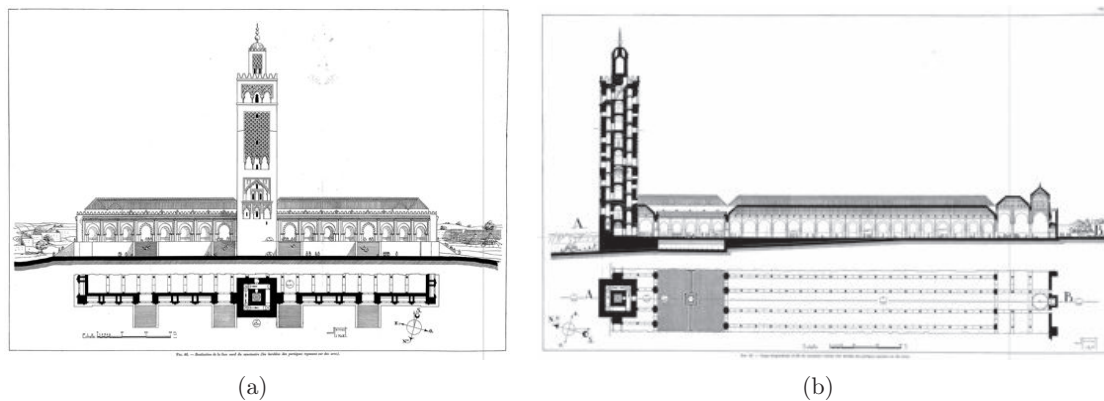


FIGURE 6 – Two examples of plans from [7] (see the electronic document for good quality).

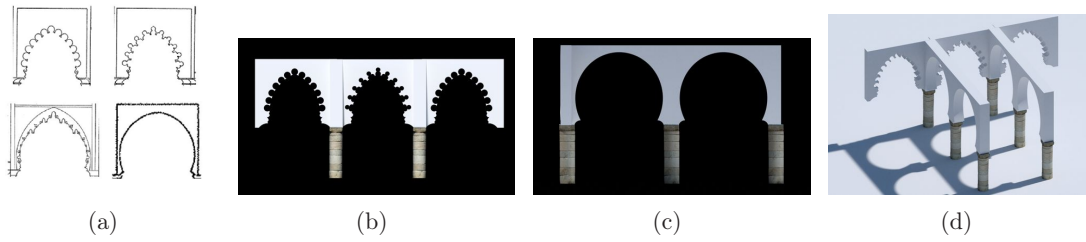


FIGURE 7 – (a) Restitution of the arches . (b) (c) (d) 3D reconstruction of all arches.



FIGURE 8 – (From left to right) Different steps of 3D reconstruction of outer wall.

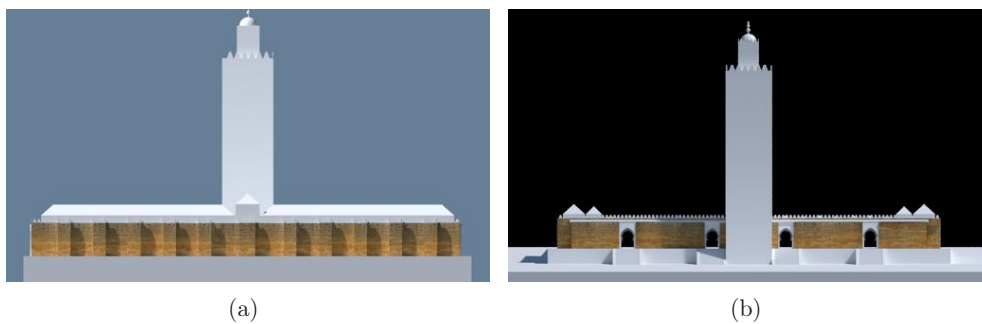


FIGURE 9 – Final 3D reconstruction of the outer wall.

The final model of the mosque includes all the parts mentioned above. The parts that appear several times in the plans are duplicated with the Blender Array modifier according to the distances in the plans. The parts that appear once as the minaret are added directly to the final model of the mosque. For example, to duplicate the arcs and the pillars we used several plans and especially the top view and cutplanes (Fig. 6) of the mosque from [7]. Fig. 11 shows the top view and the same view in final 3D reconstruction of the mosque.

Fig. 12 gives a view without the roof in order to show the global structure of the mosque and a global perspective view.

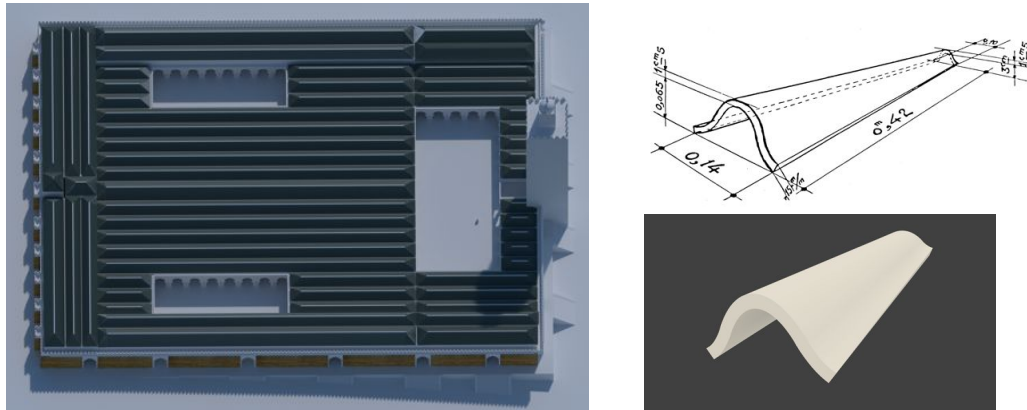


FIGURE 10 – (a) 3D reconstruction of the roof. (b) Tile shape and dimension [7]. (c) 3D model sample of the tile.

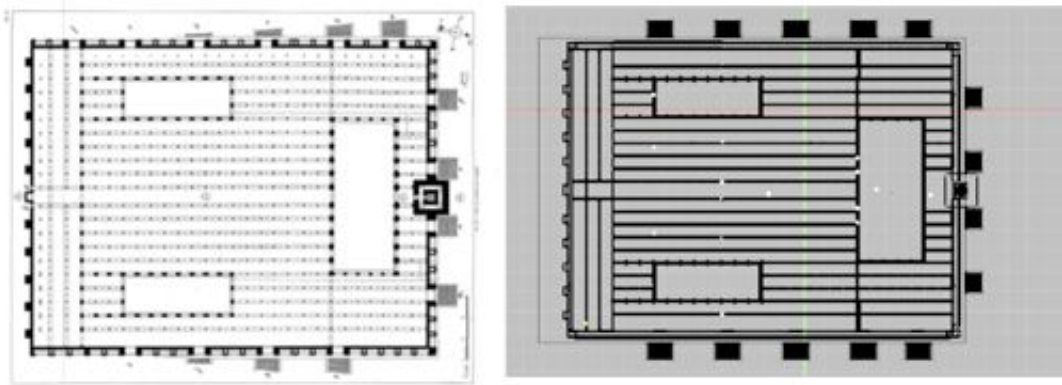


FIGURE 11 – At left plan of top view of the mosque[7]. At right top view of 3d reconstruction of the mosque.

4. Complete 3D model and comments on the architecture of the Hassan mosque

Hassan Mosque stands for a very moving monument due to its proportions and perfect design as we can see in Fig. 11 and Fig. 12 for a view with and without roof. The mosque was conceived to be the vastest worship space of the whole western medieval Muslim community and the most outstanding monument of Almohade dynasty. It covers an area of 25551 square meters, in a quadrilateral shape 185 meters long and 140 meters width and surrounded with a wall in Tabya (pisé). The enclosure is punctuated with square bastions giving to it a military

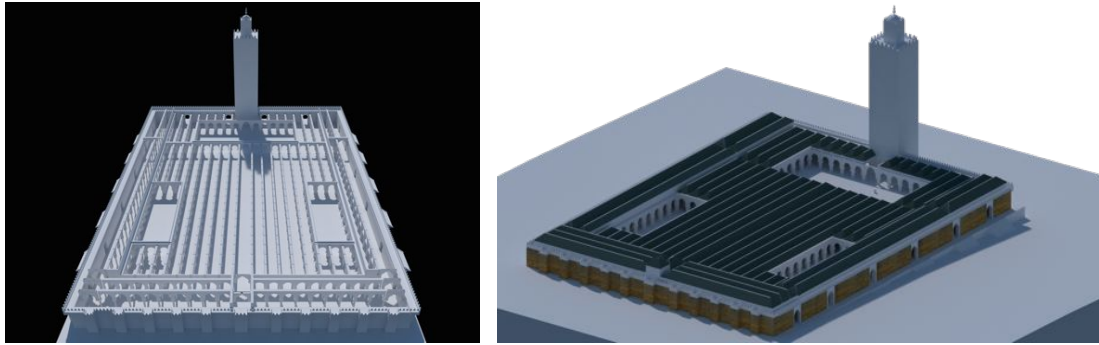


FIGURE 12 – Views of the final 3d reconstitution of the Hassan mosque in Rabat.

appearance; a new trend adopted by Almohades for worship spaces to symbolize their faith as well as their power. Many gates give access to the huge building : six of them are on the south-west side. The Northeast and North-West sides are open via four bays each Fig. 11. Salient canopies top these doors. These are allowing access to a large prayer hall almost square shaped. The naves are marked off by lined up rows of columns compound of cylindrical drums. The naves are perpendicular to the Qibla wall. These are set up in odd number on either side of a wider and taller axial nave. The intersection of this and the transept nave (the qibla nave) having the same dimensions, delimit a square area that receives a dome, the principal function of which is to enhance the Mihrab alcove (believers commander place), as it is usual in earlier Oyemade's, Aghlabids' and Almoravides Mosques. In this vast prayer hall, one can distinguish two specific areas : the first running along the qibla wall, which counts three parallel naves, and the second, more spacious, made of twenty-one naves perpendicular to those of the first area. The median naves, those of the qibla and those that are lateral are the same width. The first naves create the plane in **T**, the others lead to the plane **U**. To assure good airing and enough lighting to the monument grouping, Hassan Mosque is equipped on both sides of the longitudinal axis of two secondary courtyard barlongue shaped Fig.12. This plane with perfect symmetry where « shows a perfect predilection to the square is an unusual fact ([8], p. 207). However, to be different from their predecessors, Almohade master-builders introduced some innovations. The first innovation in the increasing number of domes in the transept nave that is competing with the axial nave. The two lateral naves of prayer halls are enlarged to obtain the same width as that of the transept nave and hence to keep, in both ends of this, two squared areas bearing two new domes like in Taza and Tinnel grand mosques. Besides this disposal, Hassan Mosque is made up of an uncovered courtyard : the Sahn (Fig. 12), bearing a rectangular shape (71, 50 meters of width and 27 meters in depth). This courtyard is organized in a perfect mouminide tradition reminding of Tinnel, Taza or Koutoubiya courtyard. Hassan mosque Sahn grows longer on both sides with two galleries in continuation of lateral naves of the oratory. In the center of north wall, there is a minaret/tower, reminding by its location, the minaret of Sidi Ukba Mosque in Kairouan. The buttress towers of its southern façade testify the influence of Cordoue Mosque. The northern façade is composed of three superimposed naves; the first one spreads out a polyfoiled arc bordered with two arcs the springing of which are made of thin columns in white marble. The next alcove raises the first one, and shows a big arc holding tightly three polyfoiled arcs. The last register covers the truncated part of the façade. Three polyfoiled arcs are used on flat end on which rests an intertwine diamond shaped and curved darjel ktef. For a symmetry purpose, the same intertwine resting on the same type of arcs to fill out the upper register of the southern façade. The lower register of this is showing a worn out arc overstepping

with smooth horses wrapped up by a large arc the extrados of which shows nine arcs with seven foils. The register axis is characterized by twin blind alcoves in form of pelmet arcs topped with a network of diamonds and two-headed curves. Eastern and western façades are reproducing almost the same composition. This is repeating a diamond frame in curved mesh supporting on either side three foil arcs similar to those already met on the same level of the northern façade.

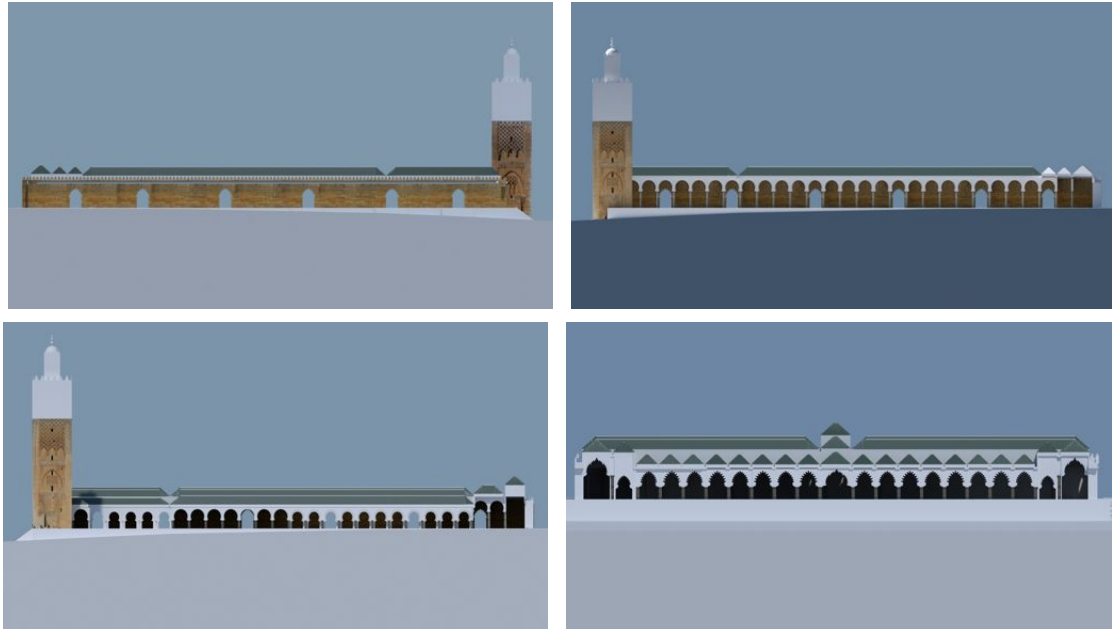


FIGURE 13 – Longitudinal views.

5. Conclusion

In the aim to preserve the Moroccan architectural cultural heritage, we focus on the famous historical monument : the Hassan mosque. Our goal is to give the complete digital 3D model of what the Hassan mosque was supposed to be if its construction was finalized and remain intact. We have combined digitization techniques based photogrammetry and laser scanner to obtain the exact geometry, texture and color for the existent parts of the mosque. To complete the 3D model, we have used historical sources and archives to reconstruct the inexistent part of the mosque using Blender. We have succeeded restitution of five important parts of this huge mosque. This restitution is conforming to the plans given in [7] and allows to provide a realistic global structure of the mosque. Nevertheless, the obtained 3D model remains incomplete. We intend to explore other sources and archives in order to complete the restitution of the other inexistent parts of the Hassan mosque. On the another hand, we will develop some tools to allow the 3D navigation in this model.

The work whose premises have been presented in this paper, are intended to continue. We hope they will arouse a renewed interest in this monument.

Acknowledgements

The authors would like to thank the PhC Toubkal.

Références

- [1] <https://mis.u-picardie.fr/e-cathedrale/>.
- [2] K. Ait El Kadi. *Extraction des éléments des façades des bâtiments du patrimoine architectural à partir de données issues de scanner laser terrestre*. In PhD Thesis - Institut Agronomique et Vétérinaire Hassan II, 2016.
- [3] N. Crombez, G. Caron, E. Mouaddib. *3D point cloud model colorization by dense registration of digital images*. In 3D Virtual Reconstruction and Visualization of Complex Architectures, 3DARCH, ISPRS workshop, Feb 2015, Avila, Spain.
- [4] M. Kazhdan, H. Hoppe. *Screened poisson surface reconstruction*. In ACM Transactions on Graphics (TOG), 2013, vol. 32, no 3, p. 29.
- [5] <http://pointclouds.org/>
- [6] M. Dieulafoy. *La Mosquée d'Hassan*. Extrait Des mémoires de l'académie des inscriptions et belles-lettres, tome XLII, 1920.
- [7] J. Caille. *La Mosquée de Hassan à Rabat*. Publishing Editor, Number of Pages, Year of Publications.
- [8] G. Marcais. *Manuel d'art musulman. L'architecture*. 2 vol. Paris, 1926 et 1927.
- [9] E. Rupnik, M. Daakir, and M. Pierrot Deseilligny, *MicMac – a free, open-source solution for photogrammetry*, In Open Geospatial Data, Software and Standards, 2017.

Instructions for authors

1. Type of Manuscripts
2. Organization of the Manuscript
3. Language
4. Submission of the Manuscript
5. Peer Review
6. Revision of the Manuscript
7. Special Features, Appendices and Supplementary Material
8. Preprint Option
9. Publication of the Manuscript

Frontiers in Science and Engineering an International Journal edited by Hassan II Academy of Science and Technology uses author-supplied PDFs for all online and print publication.

1. Type of Manuscripts

The FSE Journal publishes the following article types :

Reviews/State of the art, usually through Academy invitation and organized into themed issues, report on recent advances in science and technology. 20 pages maximum according to the format given.

Original Research Papers contain innovative and hypothesis-driven research; supported by sound experimental design, methodology, proofs, and data interpretation. 16 pages maximum according to the format given.

Letters to the Editor: May be submitted by readers commenting articles already published by the Journal. 1 to 2 pages maximum according to the format given.

2. Organization of the Manuscript

The entire manuscript, including mathematical equations, flow-sheets, chemical structures, tables, and figures must be prepared in electronic form and submitted as pdf files. Use Times New Roman size 12. For all special characters (e.g., Greek characters) use the font Symbol. Use carriage returns only to end headings and paragraphs, not to break lines of text. Automatic hyphenation should be turned off. Do not insert spaces before punctuation. Verify the correct spelling for the final version with the Spelling and Grammar function of Word.

3. Language

Manuscripts should be written in English.

4. Submission of the Manuscript

The manuscript and supplementary material must be send by the corresponding author to the Editor in an electronic form as pdf files.

You may be required to register as a new user within the Publication System Manager upon your first visit. Straightforward login and registration procedures can be found on the website. Editorial Manager allows authors to track the progress of manuscript review in real time. Detailed, step-by-step instructions for submitting manuscripts can be found on the website. All correspondence regarding your manuscript must go through Publication System Manager.

Authors are asked to prepare their papers, and PDF files, according to the templates and guidelines provided below.

The author(s) need to supply the following items :

- the PDF file of the paper
- a signed Assignment of Copyright Form (once the paper accepted)

We highly recommend that authors prepare their papers/PDFs using the following Microsoft Word or LaTeX templates, which can be downloaded from the following links :

- Microsoft guidelines and templates
- Latex guidelines and class file

A copyright license form will be provided to the corresponding author only when a paper is accepted for publication.

5. Peer Review

All submissions will be reviewed anonymously by at least two independent referees, and a referee should never communicate directly with an author. A referee must treat as confidential material the manuscript and any supplementary material. Authors may suggest names and email addresses of expert reviewers, but selection remains a prerogative of the Editors. Authors may include supplementary notes to facilitate the review process. If an accepted paper is cited

that has not yet appeared in print and is required for evaluation of the submitted manuscript, authors should provide an electronic version for use by the Reviewers. Authors are responsible for all statements in their work, including changes made by the copy editor after a manuscript is accepted.

6. Revision of the Manuscript

All comments made by referees must be addressed. A letter describing all changes that were made should be attached with the revised version of the manuscript. A copyright license form must accompany the final version of the manuscript.

7. Special Features, Appendices and Supplementary Material

Special features containing highly interactive features or large databases can be included. All authors are encouraged to take advantage WEB online publishing capabilities (i.e. 3-D, video, and interactive graphics). All special features must be created by the Author(s).

Authors who wish to publish electronic supplementary material to their article (Excel files, images, audio/video files) must submit the supplementary files/materials with their manuscript submission via our online peer review tracking Publication System Manager. Note that supplementary files are not automatically included in the reviewer PDF. Please therefore note in the cover letter if these materials should be evaluated by reviewers.

8. Preprint Option

Before making a PDF file of your article, please check the following tips in the next section.

Article checklist

There are a number of essential basic requirements which must be followed during preparation of your article. If article PDFs are prepared without following these essential requirements, publication may be delayed until a usable and compatible PDF is received.

Articles must not contain page numbers, headers or footers

This is extremely important. Page numbers, copyright details etc are added by the Publication System Manager Publishing during the production and publication process. If you put page numbers on your paper we will have to contact you for a replacement PDF, which could delay publication.

Article margins must be adequate

We recommend a minimum 15mm all round. The Microsoft Word template or Latex templates automatically provide the correct margins so their use is highly recommended.

All articles must have an abstract

When readers are searching for information online, an abstract of an article is the first thing they see. Your abstract needs to be concise but convey as much information as possible about the content of your article. In addition, our Publication System Manager Publishing will supply your abstract to many other database systems used by researchers to find papers.

Addresses should be complete and include the country and a contact name

The title of the article, author names with full first name (no degrees), each author's affiliation, and a suggested running head (of less than 50 characters, including spaces). The affiliation should comprise the department, institution (usually university or company), city, and country and should be typed as a footnote to the author's name. For the corresponding author designated to correspond with the Editorial Office and review proofs, indicate his/her complete mailing address, office/cellular telephone number, fax number, and e-mail address. During production of the electronic paper we may need to contact you if there is something to check or for a request a replacement PDF file.

References should be complete and carefully formatted

Online versions of all reference lists will, wherever possible, be electronically linked to the articles that you cite. Reference lists containing many links direct to the cited paper are a valuable research tool. The time and effort spent in preparing your references, so that they can be linked, will be very appreciated by readers of your paper. Please, notice also that all the citations should be justified according to the contents of the proposed article. Abusive citations of the same author may induce a certain delay in the overall review process

PrePrint

Any manuscript received for publication in FSE can be published on the Web as preprint. All authors submitting a manuscript must clearly indicate that they wish to publish it as a preprint. The referees appreciate if the manuscript meets the basic requirements for publication and recommend its publication as preprint. A preprint not accepted for publication by the referees will be immediately removed from the preprint collection. A published paper which was previously available as a preprint will have clearly indicated the date when it was first published on the Web. A work published as preprint can benefit from comments from the readers which can eventually improve the manuscript. Revised versions that incorporate corrections from reviewers and suggestions from readers can be also published as preprints.

9. Publication of the Manuscript

Accepted papers are published as PDF files available at the Web site of the Academy.

Transfer of Copyright Form

A signed copy of the Transfer of Copyright must be submitted online as part of the manuscript submission process (FSECopyright.pdf).

Abstract

Reviews/State of the Art, Original Research Articles, require an abstract. The abstract is limited to 300 words or less. For Research Articles, the abstract should include a brief statement for each of the sections related to Introduction, Methods/Approaches/Materials and Discussion, and Conclusion written in paragraph form. All abstracts must be written in one paragraph, with no subheadings, equations, tables, reference citations or graphics.

Keywords

Provide a list of no more than 5 key words.

Introduction

Required for Reviews/State of the art and Original Research Articles.

Main Text Body

For Original Research Articles, organize the main text as follows: Introduction, Approach/Materials and Methods, Results, Discussion, and Conclusion. The use of subheadings to divide the text is encouraged. Primary, Secondary, and Third level headings should be clearly defined, but do not use numbers or letters.

Recommended word counts are as follows: Reviews/State of the art: 8000, Original Research Articles : 6000.

Use abbreviations sparingly, and define them at the first insertion in the text. Use the metric system for all measurements. Express metric abbreviations in lowercase letters without periods (cm, ml, sec). Define all symbols used in equations and formulas. When symbols are used extensively, the authors may include a list of all symbols in a table.

Conclusion

The conclusion should be a brief paragraph, containing 3 to 4 sentences, that summarizes the findings presented.

Acknowledgments

Include funding source(s) and other contributions. If the work has been funded by any organisation please provide name(s) of funding institute(s) and grant number(s).

References

References should conform to Vancouver style and be numbered consecutively in the order in which they are cited in the text. Cite in the text by the appropriate Arabic numeral enclosed in parentheses, e.g., (1), (2-5), etc.

It is advisable to limit the maximum number of references as really needed only.

References to unpublished peer-reviewed, personal communications, including conference abstracts, and papers in preparation or in review, cannot be listed, but can be notated parenthetically in the text.

Abbreviations for journal names should conform to those of Vancouver style (as depicted in <http://www.library.uq.edu.au/training/citation/vancouv.pdf>). The style and punctuation of the references should conform to conventional referencing.

Whenever, the paper is not yet published officially but accepted, please write down the corresponding DOI within the reference.

Authors may identify uniform resource locators (URLs) for websites that provide the reader with additional information on the topic addressed in the manuscript. Although URLs are an important feature of electronic publishing, authors are encouraged to be very selective in their choice of sites to include. Do not include links to sites that are not accessible without a password.

All on-line documents should contain author(s), title, On-line document/ Web /FTP /organisation /On-line database/ Supplementary material/ Private homepage , and Accessed Day Month Year, so that readers can refer to.

Tables

Tables must be created in Microsoft Word /Latex table format. Tables should be numbered (with Roman numerals) and referred to by number in the text. Center the title above the table, and type explanatory footnotes (indicated by superscript lowercase letters) below the table. Data must be placed in separate cells of the table to prevent text and numbers from shifting when the table is converted for publication on the Internet. Empty cells may be inserted to create spacing. Tables should not duplicate information provided in the text. Instead, tables should be used to provide additional information that illustrates or expands on a specific point the author wishes to make. Each table should be self-explanatory.

Figures

The FSE offers authors the use of color figures in online published manuscripts. Figures (as well as photographs, drawings, diagrams, and charts) are to be numbered in one consecutive series of Arabic numerals in the order in which they are cited in the text. All Electronic artwork must be submitted online via our online peer review tracking system, Publication System Manager.

The maximum combined count for tables and figures for papers should not exceed 15 to 20.

Footnotes

Footnotes should be avoided. When their use is absolutely necessary, footnotes should be numbered consecutively using Arabic numerals and should be typed at the bottom of the page to which they refer. Place a line above the footnote, so that it is set off from the text. Use the appropriate superscript numeral for citation in the text.

Guidelines

We highly recommend that authors prepare their papers/PDFs using the following Microsoft Word or LaTeX templates, which can be downloaded from the following links:

- Latex guidelines and class file <http://www.academie.hassan2.sciences.ma/fse/FSE%20Sample%20cls.tex.txt>
- PDF guidelines and templates <http://www.academie.hassan2.sciences.ma/fse/FSE%20Sample%20cls.pdf>
- Microsoft word guidelines and templates

Contractual issues

1. Full Disclosure

During the manuscript submission process, all authors will be required to confirm that the manuscript has not been previously published in any language anywhere and that it is not under simultaneous consideration by another journal.

2. Conflicts of Interest

Authors must declare all conflicts of interest (or their absence) in their cover letter upon submission of a manuscript. This conflict declaration includes conflicts or potential conflicts of all listed authors. If any conflicts are declared, FSE publish them with the paper. In cases of doubt, the circumstance should be disclosed so that the editors may assess its significance.

Conflicts may be financial, academic, commercial, political or personal. Financial interests may include employment, research funding (received or pending), stock or share ownership, patents, payment for lectures or travel, consultancies, nonfinancial support, or any fiduciary interest in a company.

3. Copyright Transfer

The Copyright Revision Act requires that Authors transfer their copyrights to the Publisher, HIIAST, in order to provide for the widest possible dissemination of professional and scientific literature. A signed Transfer of Copyright form must be submitted online with the manuscript. The Transfer of Copyright form for an accepted manuscript must be on file with the HIIAST Editorial Office prior to production for publication. Corresponding Authors may print and sign the form on behalf of all authors. The Transfer of Copyright form can be found at [fsecopyright.pdf](#).

4. Use of Copyrighted Tables and Figures

A copy of the granted permission to use copyrighted figures and tables must be included with the submitted manuscript.

